JGR Atmospheres

RESEARCH ARTICLE
10.1029/2018JD029842

Multiple-Wavelet Coherence of World's Large Rivers With Meteorological Factors and Ocean Signals

Lu Su[1], Chiyuan Miao[1], Qingyun Duan[1], Xiaohui Lei[2], and Hu Li[3]

[1]State Key Laboratory of Earth Surface Processes and Resource Ecology, Faculty of Geographical Science, Beijing Normal University, Beijing, China, [2]State Key Laboratory of Simulation and Regulation of Water Cycle in River Basin, China Institute of Water Resources and Hydropower Research, Beijing, China, [3]Key Laboratory of Agricultural Non-point Source Pollution Control, Ministry of Agriculture/Institute of Agricultural Resources and Regional Planning, Chinese Academy of Agricultural Sciences, Beijing, China

Key Points:
- Significant annual streamflow oscillations occurred in 16 world's large rivers
- We identified the multivariate relationships between streamflow and predictors
- The combinations of factors that best explained streamflow variations are different

Correspondence to:
C. Miao,
miaocy@vip.sina.com

Citation:
Su, L., Miao, C., Duan, Q., Lei, X., & Li, H. (2019). Multiple-wavelet coherence of world's large rivers with meteorological factors and ocean signals. *Journal of Geophysical Research: Atmospheres*, *124*. https://doi.org/10.1029/2018JD029842

Received 16 OCT 2018
Accepted 7 APR 2019
Accepted article online 16 APR 2019

Abstract Streamflow is controlled by multiple factors concurrently. However, the multivariate relationship between global streamflow and meteorological factors/ocean signals is rarely explored at different temporal scales. Determining a suite of factors that explain most of the variations in global streamflow at multiple scales will be of great significance for water-resource management and prediction. Temporally dependent multivariate relationships between streamflow and meteorological factors/ocean signals in 16 of the world's large rivers were identified using wavelet transform coherence and multiple-wavelet coherence. Prior to that, the continuous wavelet transform was used to detect temporal patterns in streamflow. The continuous wavelet transform results showed that significant annual oscillations occurred in all streamflow series over the study period, either with continuous annual periodicity or with intermittent breaks. Oscillations with periodicities of around 4 to 6 months were also found in many rivers. A comparison of the results from the wavelet transform coherence and multiple-wavelet coherence analyses indicated that streamflow variation could be best explained by one, two, or three meteorological factors. The combination of factors that best explained streamflow variations differed among the rivers, although total precipitation (PRE) or the number of rainy days (WET) either alone or in combination was a dominant factor for all rivers. The most common best predictor was PRE or/and WET combined with potential evapotranspiration. The differences in best predictor were due to differences in latitude, radiation forcing, terrain, vegetation coverage, hydrological processes, and so forth.

1. Introduction

Water is essential for survival. Rivers, being the main source of freshwater on land, are vital for human health, economic activities, ecosystem function, and geophysical processes. As the world's population continues to grow, water scarcity is accelerating across the globe (Arnell, 1999; Bogardi et al., 2013). Therefore, the changing characteristics and long-term trends in river flow have received great attention in recent decades, especially with regard to the changing climate (Arnell & Lloyd-Hughes, 2014; Haddeland et al., 2014; Oki & Kanae, 2006; Schewe et al., 2014; Vorosmarty et al., 2000). Substantial research effort has been focused on fluctuations in streamflow (Kong et al., 2015; Miao & Ni, 2009; Yang et al., 2017).

River flow is determined by the amount of precipitation minus the amount of water lost through evapotranspiration and is also affected by changes in storage, including as snow, ice, and groundwater, and by human activities, including reservoir interception and water diversion (Yang et al., 2016). However, the effects of water withdrawals and dams appear to be significant only for arid to semiarid river basins such as the Indus, Yellow, and Tigris-Euphrates basins (Milliman et al., 2008), and climate forcing predominates for most of world's large rivers (Dai et al., 2009). Increased storage of water in reservoirs and water withdrawals are compensated for by groundwater mining, urbanization, and the effects of deforestation (Dai et al., 2009). The net sum of land effects is now thought to be small (Dai et al., 2009; Domingues et al., 2008; Ngo-Duc et al., 2005). In addition, the effect of dams on streamflow is mainly seasonal; we consider the coherence of streamflow and predictors at all time scales, which therefore also minimizes the effect of dams on our results (Dai et al., 2009; Döll et al., 2009). Precipitation is the main driver of global streamflow trends and interannual variability in most regions (Iles & Hegerl, 2015). Evapotranspiration plays a crucial role in global climate change and in the hydrological cycle (Wang et al., 2006; Yang et al., 2019). In the overwhelming majority of populated regions in the world, the proportion of precipitation lost to evapotranspiration is

greater than that ends up as runoff (Wang et al., 2006). As well as affecting evapotranspiration, changes in temperatures also influence streamflow via changes in the accumulation and ablation of snow and ice.

Substantial research has therefore focused on the relationship between streamflow and meteorological factors. Arnell (1999) examined the effect of different climate-change scenarios on simulated global river flows using a macroscale hydrological model. They predicted that river runoff would decrease in many areas of the world owing to reduced precipitation over large regions of land coupled with an increase in evaporative demand associated with higher temperatures. Milliman et al. (2008) detected the cumulative annual discharge from 137 representative rivers over the last half of the twentieth century and found that the discharge trends for many rivers generally reflected changes in precipitation, which were primarily due to fluctuations in short- and longer-term atmospheric-oceanic signals. Gerten et al. (2008) used a global vegetation and hydrology model (LPJmL) to quantify the factors contributing to river discharge and found that total global discharge rose over the period 1901–2002, primarily because of increased precipitation, global warming, rising CO_2 levels, and changes in land cover. McCabe and Wolock (2011) generated a monthly runoff data series for global land areas for the period 1905–2002 using a monthly water-balance model with CRUTS2.1 monthly temperature and precipitation data. They found that, even though annual precipitation accounted for most of the temporal and spatial variability in annual runoff, increases in temperature have had an increasingly negative effect on annual runoff since 1980. Increased temperatures cause a reduction in the fraction of annual precipitation that becomes runoff (i.e., a reduction in runoff efficiency) owing to increases in evapotranspiration. Tang and Lettenmaier (2012) estimated the runoff response to the changes in global mean temperatures indicated by climate change experiments. The estimated ratio of runoff change to (local) precipitation change (runoff elasticity) ranged from about one to three, and the runoff-temperature sensitivity (change in runoff per degree of local temperature increase) ranged from decreases of about 2% to 6% over most basins in North America and in the middle and high latitudes of Eurasia. Arnell and Gosling (2013) used a global hydrological model to assess the impact of climate change on a series of hydrological-regime indicators. They found considerable variability between regions, largely due to differences in the projected changes in precipitation. Beck et al. (2015) used observed streamflow from 3,000 to 4,000 small-to-medium-sized catchments located across the world to train neural network ensembles to estimate streamflow characteristics from climate data and the physiographic characteristics of the catchments. Overall, climate indices, including precipitation and evapotranspiration, dominated among the predictors (Beck et al., 2015).

The global hydrological cycle consists of water in the oceans, the atmosphere, and the landscape (David, 2010; Oki et al., 2004; Trenberth et al., 2007). As a main component of the hydrological cycle, river streamflow is influenced by complex ocean-atmosphere interactions. Ocean-atmosphere oscillations tend to be strongly correlated with river streamflow and hence provide valuable information for hydrological forecasting (Wanders & Wada, 2015). Indices describing coherent patterns of large-scale ocean-atmosphere oscillations, such as the Arctic Oscillation (AO), the North AO (NAO), the Southern Oscillation Index (SOI), Niño 3.4—the Pacific mean sea-surface temperature (SST), the Dipole Mode Index (DMI), and the Pacific Decadal Oscillation (PDO), act as convenient and relatively effective predictors of streamflow variability (Fleming & Dahlke, 2014).

Several studies have examined the effects of these climate oscillations on river flow worldwide, though most focused on the effects of the El Niño-Southern Oscillation (ENSO) and changes at the annual time scale and most were limited to specific regions of the world (Wanders & Wada, 2015). For example, Chiew and McMahon (2002) reported clear ENSO-streamflow teleconnections in an analysis based on two ENSO indicators. David (2010) used a cross-wavelet analysis to detect the relationships between estimated annual continental freshwater discharge and selected climate indices (NAO, AO, SOI, PDO, and Niño 3.4) over the period 1876–1994 and found highly temporally nonstationary relationships with three main bands of variability (2–10, 10–20, and 20–30 years). Wanders and Wada (2015) showed strong correlations between the NAO, the AO, or the PDO and modeled and observed global discharge anomalies over a 100-year period.

Large rivers are an essential water resource for the surrounding living beings and are the sources of human civilization. A large amount of research on the relationship between streamflow and various predicting factors has been performed on large rivers around the world, for example, on the relationships between meteorological factors/ocean signals and streamflow in the Amazon river (Davidson et al., 2012; Espinoza Villar et al., 2009; Kitoh et al., 2011; Marengo et al., 2011; Zeng et al., 2008), the Yangtze river (Changjiang river;

Wei et al., 2014; Xu et al., 2007, 2010; Zhang et al., 2014), the Mississippi river (Massei et al., 2011; Salas et al., 2011; Tootle et al., 2005; Twine et al., 2005), the Mekong river (Cook et al., 2012; Costa-Cabral et al., 2008; Fan & He, 2015; Lutz et al., 2014), the Ob river (Shiklomanov et al., 2007; Shiklomanov & Lammers, 2014; Surazakov et al., 2007), and so forth.

Nevertheless, existing research has mostly focused on streamflow within individual rivers, and the relationships assessed have been mainly limited to two variables (e.g., Marengo, Tomasella, Alves, et al., 2011; Salas et al., 2011; Shiklomanov et al., 2007; Zeng et al., 2008; Zhang et al., 2014). A comprehensive study of the world's large rivers will thus contribute to a better understanding of global hydrology. Hydrological processes are intricate and are usually influenced by multiple factors. Measuring the effect of a single factor (such as precipitation) alone will not fully capture all the features of the processes. Thus, it is essential to study multivariable coherence to better reveal the salient features of the underlying processes at specific temporal scales.

Several methods can be used to detect multivariate relationships, for example, multiple spectral coherence (Si, 2008), a combination of multivariate empirical mode decomposition and the squared multiple correlation coefficient (MCC_{memd}; Hu & Si, 2013; She et al., 2016), and trivariate cross-wavelet spectral analysis (Mihanović et al., 2009). However, multiple spectral coherence requires a stationary data series, which is rare in hydrology (Hu & Si, 2016) since hydrometeorological signals arise from physical processes that operate over a large range of scales varying from 1 day to several decades (Yu et al., 2015). With regard to MCC_{memd}, the total variance in the original series typically does not equal the sum of the variances of the different components, which may lead to false results (Hu & Si, 2016). Furthermore, multivariate relationships in hydrology are most likely to be transient and inhomogeneous. Scale- and/or location-dependent information are not available with the above multivariate methods (Hu & Si, 2016). Trivariate cross-wavelet spectral analysis is only applicable to two orthogonal predictor variables, which limits its applicability in the geosciences where there are commonly more than two predictor variables and where the variables are often cross-correlated.

As the traditional multivariate methods fail to capture scale-specific, localized information and ignore the correlations between predictor variables, these methods may identify redundant predictor variables and thus prevent us from finding the most efficient way to explain the variations in the response variable (Hu et al., 2017). To overcome the disadvantages of the existing multivariate methods, Hu and Si (2016) developed multiple wavelet coherence (MWC). MWC can untangle a range of multivariate relationships: It is able to identify spatial or temporal scale multivariate relationships, and it can be used to determine the proportion of the variance associated with a response variable that is explained by predictor variables, at specific spatial or temporal scales. Hu et al. (2017) used bivariate wavelet coherency and MWC to explore the spatial scale- and location-dependent multivariate relationships between soil water content and environmental factors in a hummocky landscape in North America. Their study showed that MWC is an effective method for untangling the complex spatial and temporal variability associated with multiple controlling factors at multiple scales and led to an improved understanding of the underlying hydrological processes.

MWC is therefore conducive to proper characterization of the temporal scale-specific multivariate relationships between global streamflow and predicting factors. A good understanding of these relationships is important for optimizing the variables used in temporal scale-dependent predictions of global streamflow. Specifically, it is important in global climate modeling to determine the dominant factors influencing streamflow in order to be able to project realistic and meaningful changes in streamflow. Existing large complex system models have not been able to fully simulate global streamflow. Clarifying the most prominent factors influencing global river streamflow will improve the accuracy of model simulations. Here we present a systematic method for isolating the most important factor combinations, which is a crucial first step in climate modeling involving hydrological responses. Before detecting the multivariate relationships, the dominant modes of streamflow variability and how such modes vary with time can be determined by one-dimensional wavelet analysis (Torrence & Compo, 1998); the transient associations between the two nonstationary variables in both the time and frequency domains can be studied by bivariate wavelet transform (Yu et al., 2015).

The main aim of this study is to analyze the relationships between streamflow in large rivers across the world and various meteorological factors and atmospheric drivers. First, the continuous wavelet transform (CWT)

Table 1
River Information

River	Station	Country	Period	Length (km)	Length ranking[a]
Amazon	Obidos	Brazil	1928–2013	6,400	2
Yangtze	Datong	China	1900–2016	6,300	3
Mississippi	Vicksburg	United States	1928–2013	5,900	4
Ob	Salekhard	Russia	1930–2010	5,400	6
Mekong	Timbues	Vietnam	1923–2012	4,800	7
Congo	Kinshasa	Congo	1903–2010	4,700	9
Lena	Kusur	Russia	1934–2011	4,400	10
Amur	Komsomolsk	Russia	1900–2006	4,400	11
Mackenzie	Arctic Red	Canada	1943–2013	4,200	12
Yenisei	Igarka	Russia	1936–2011	4,100	13
St. Lawrence	Cornwall ON	Canada	1900–2013	4,000	14
Niger	Lokoja	Nigeria	1915–2012	4,000	15
Yukon	Pilot Stn	United States	1956–2013	3,700	16
Danube	Ceatal Izmail	Romania	1900–2010	2,900	21
Tocantins	Tucurui	Brazil	1955–2014	2,700	24
Nelson	u/s Bladder	Canada	1915–2011	2,700	25

[a]Length Ranking from Milliman and Farnsworth (2011)

is applied to detect temporal patterns in the streamflow. Second, the wavelet transform coherence (WTC) between streamflow and each predicting factor is calculated. Then, the MWC between streamflow and every combination of two or more factors is determined. Finally, we compare the percentage of streamflow variation explained by each factor to identify the dominant factors.

2. Data

2.1. Streamflow Data

Delineating the teleconnections between streamflow and ocean signals ideally requires a 50- to 100-year streamflow record that covers the time span of short-term ocean signals such as the NAO or ENSO and longer cycles such as the PDO. Unfortunately, of the 925 rivers that discharge directly to the ocean, as listed in the Dai and Trenberth Global River Flow and Continental Discharge Dataset, and of the ~650 rivers listed in the Global Runoff Data Centre (GRDC), only a few records span the entire twentieth century. Therefore, we chose 16 large rivers in the world that have full records spanning from ~60 to ~110 years in length.

The streamflow data were obtained from the Dai and Trenberth Global River Flow and Continental Discharge Dataset (http://www.cgd.ucar.edu/cas/catalog/surface/dai-runoff/index.html) and from the Global Runoff Data Centre (http://www.bafg.de/GRDC/EN/Home/homepage_node.html). Dai (2016) found that the basin-averaged water-year (October–September) mean Palmer Drought Severity Index, precipitation, and model simulated runoff (from Dai et al., 2009, for 1948–2004 only) were often highly correlated with observed streamflow (with correlation coefficient $r \approx 0.4$–0.9); thus, he used one of these (the one with the highest r) to fill in data gaps in the water-year streamflow data series through linear regression. We used monthly observed streamflow data ranging from 1900 to 2014. After data filing, streamflow records were incomplete for many rivers. We therefore checked the data and excluded rivers that had more than 1% missing values. Ultimately, we used data from 16 large rivers with records spanning from ~60 to ~110 years (Table 1).

2.2. Meteorological Factors and Ocean Signals

The AO index is calculated as the projection of monthly mean 1,000-mb height anomalies onto the first empirical orthogonal function mode poleward of 20°N, using reconstructed data from the twentieth century. The NAO is traditionally defined as the normalized pressure difference between a station on the Azores and one on Iceland. The Niño 3.4 index and the SOI are representative indexes for the ENSO. The Niño 3.4 index is the area-averaged SST from 5°S–5°N and 170–120°W over the Pacific (Trenberth, 1997). The SOI is defined as the normalized pressure difference between Tahiti and Darwin. The PDO is calculated from monthly SST anomalies poleward of 20°N in the Pacific basin. The DMI is the intensity of the Indian Ocean Dipole,

represented by an anomalous SST gradient between the western equatorial Indian Ocean (50–70°E and 10°S–10°N) and the southeastern equatorial Indian Ocean (90–110°E and 10°S–0°N). Monthly AO, NAO, Niño 3.4, SOI, DMI, and PDO signals were taken from the Earth System Research Laboratory from the National Oceanic and Atmosphere Administration (http://www.esrl.noaa.gov/psd/).

Monthly meteorological factors including mean temperature (TMP), total precipitation (PRE), potential evapotranspiration (PET), and the number of rainy days (WET) are calculated from high-resolution gridded data sets on a 0.5° × 0.5° grid in an area average over the upstream catchment and were obtained from the Climatic Research Unit (http://www.cru.uea.ac.uk/data/). All the meteorological factors and ocean signals cover the period January 1901 to December 2014.

3. Methods

The bivariate coherence and MWC between streamflow and the meteorological factors/ocean signals were calculated using WTC and MWC. Before the WTC and MWC can be calculated, it is necessary to first calculate the CWT.

3.1. The CWT

For a time series x_j of length N with equal sample spacing δt, the CWT $w_i(s)$ at time $t_i = i\delta t$ and scale s can be interpreted as an enhanced version of the discrete Fourier transformation $\mathrm{F}(\omega) = \sum_j x_j \exp(i\omega t_j)$ (Kaiser, 1994). The difference is that the periodic exponential $\exp(i\omega t_j)$ is substituted by a wavelet $\Psi(t_j - t_i, \mathrm{s})$ (Gedalof et al., 2004), which is a function with zero mean and localized in both time and frequency space (Grinsted et al., 2004). The wavelet function can be stretched or contracted by varying the wavelet scale s as well as translated by changing the localized time index t_i. The wavelet is analogous to a band-pass filter applied to the time series.

The time series can thus be decomposed dependent on time and scale (Maraun & Kurths, 2004):

$$W_i(s) = \sum_{j=0}^{N-1} x_j c(s) \Psi_0{}^* \left(\frac{t_j - t_i}{s} \right), \tag{1}$$

where * indicates the complex conjugate, and $\mathrm{c(s)} = \sqrt{\frac{\delta t}{s}}$ is the normalization factor that results in Ψ having unit energy. Wavelet power is defined as $|W_i(s)|^2$.

Because most practical time series are not cyclical, artifactual edge effects exist. The cone of influence (COI) is the region of the wavelet spectrum in which edge effects cannot be ignored and is defined as the e-folding time for the autocorrelation of wavelet power at each scale (Torrence & Compo, 1998).

The significance level of the wavelet spectrum is analyzed against red noise, which is an appropriate random background spectrum for many geophysical phenomena and which can be modeled as a univariate lag-1 autoregressive process (Torrence & Compo, 1998). A significance level of $p < 0.05$ is used to evaluate the statistical significance of the results.

The Morlet wavelet is a nonorthogonal, complex function and is a good choice for achieving a balance between time and frequency. It is defined as

$$\psi_0(\eta) = \pi^{-1/4} e^{i\omega_0 \eta} e^{-\frac{1}{2}\eta^2}, \tag{2}$$

where $\omega_0 = 6$ is dimensionless frequency, which provides a good balance between time and frequency localization, and η is dimensionless time (Grinsted et al., 2004; Torrence & Compo, 1998). Additional details about the CWT are given in Grinsted et al. (2004).

3.2. WTC

WTC is a correlation coefficient localized in time and frequency space, which is used to quantify the degree of linear relationship between two nonstationary series in the time and frequency domains (Cazelles et al., 2008). Given time series X and Y, with wavelet transforms $W_i^x(s)$ and $W_i^y(s)$, the wavelet coherence can be defined according to Torrence and Webster (1998) as

$$R_n^2 = \frac{\left|S\left(s^{-1}W_i^{XY}(s)\right)\right|^2}{S\left(s^{-1}\left|W_i^X(s)\right|^2\right)\cdot S\left(s^{-1}\left|W_i^Y(s)\right|^2\right)}, \tag{3}$$

in which S is a smoothing operator defined by the wavelet type used and

$$W_i^{XY}(s) = W_i^X(s)\cdot W_i^{Y}{}^*(s), \tag{4}$$

where * denotes the complex conjugate. R_n^2 takes a value between 0 and 1, where 0 indicates no correlation between the two time series and 1 indicates that the two time series are perfectly correlated with each other. The WTC reveals regions in time-frequency space where the two time series covary but do not necessarily have high power (Keener et al., 2010). In the present work, confidence levels were assessed against red-noise backgrounds. Monte Carlo methods were adopted to estimate the statistical significance of the wavelet coherence; the significance level for each scale was calculated solely from values outside the COI. A detailed description of the calculation of WTCs is provided by Grinsted et al. (2004), who note that the desirable features of WTCs come at the cost of slightly reduced localization in time-frequency space.

3.3. MWC

Assuming a response variable Y and multiple predictor variables X ($X = \{X_1, X_2, ..., X_q\}$), the MWC at scale s and location τ, $\rho_m^2(s,\tau)$, can be written as

$$\rho_m^2(s,\tau) = \frac{\underset{W}{\leftrightarrow}^{Y,X}(s,\tau)\underset{W}{\leftrightarrow}^{X,X}(s,\tau)^{-1}\underset{W}{\leftrightarrow}^{Y,X}(s,\tau)^*}{\underset{W}{\leftrightarrow}^{Y,Y}(s,\tau)}, \tag{5}$$

where $\underset{W}{\leftrightarrow}^{Y,X}(s,\tau)$ is the matrix of the smoothed cross-wavelet power spectra between response variable Y and predictor variables X; $\underset{W}{\leftrightarrow}^{X,X}(s,\tau)$ is the matrix of the smoothed auto- and cross-wavelet power spectra among multiple predictor variables X; $\underset{W}{\leftrightarrow}^{Y,Y}(s,\tau)$ is the smoothed wavelet power spectrum of response variable Y; and $\underset{W}{\leftrightarrow}^{Y,X}(s,\tau)^*$ is the complex conjugate of $\underset{W}{\leftrightarrow}^{Y,X}(s,\tau)$ (Hu & Si, 2016).

The wavelet phase between a response variable (Y) and a predictor variable (X_1) is

$$\phi(s,\tau) = \tan^{-1}\left(\mathrm{Im}\left(\underset{W}{\leftrightarrow}^{Y,X_1}(s,\tau)\right)\right) / \mathrm{Re}\,\underset{W}{\leftrightarrow}^{Y,X_1}(s,\tau), \tag{6}$$

where Im and Re denote the imaginary and real parts of $\underset{W}{\leftrightarrow}^{Y,X}(s,\tau)$, respectively.

For both the bivariate wavelet coherence and the MWC, the 95% significance level was calculated using the Monte Carlo method (Grinsted et al., 2004; Hu & Si, 2016).

3.4. Factor Identifying

The ability of different meteorological factors and ocean signals (or their combinations) to explain streamflow variation at all scales was assessed by measuring the average coherence (WTC/MWC) and the percent area of significant coherence (PASC) relative to the wavelet scale-location domain (outside the COI; Hu & Si, 2016). A greater average coherence with larger PASC indicates that more of the streamflow variation is explained by a particular predictor variable case. We focused on all scales of streamflow variation so that we could identify the factors underlying the variations in streamflow. Sometimes, the average coherence increases with an increased number of independent variables, but the PASC does not necessarily increase (Hu & Si, 2016). Statistically, an increased PASC indicates that there is a significant increase in the streamflow variations that can be explained at the 95% significant level. From a practical point of view, an additional factor is considered to be significant when it results in an increase in the PASC of at least 5% (Hu et al., 2017).

4. Results

4.1. Temporal Patterns of Streamflow

Figure 1 display the results obtained for the CWT applied to streamflow series for 16 large rivers in the world (the results of 16 rivers are shown in two parts, and the following results are shown in similar ways). The

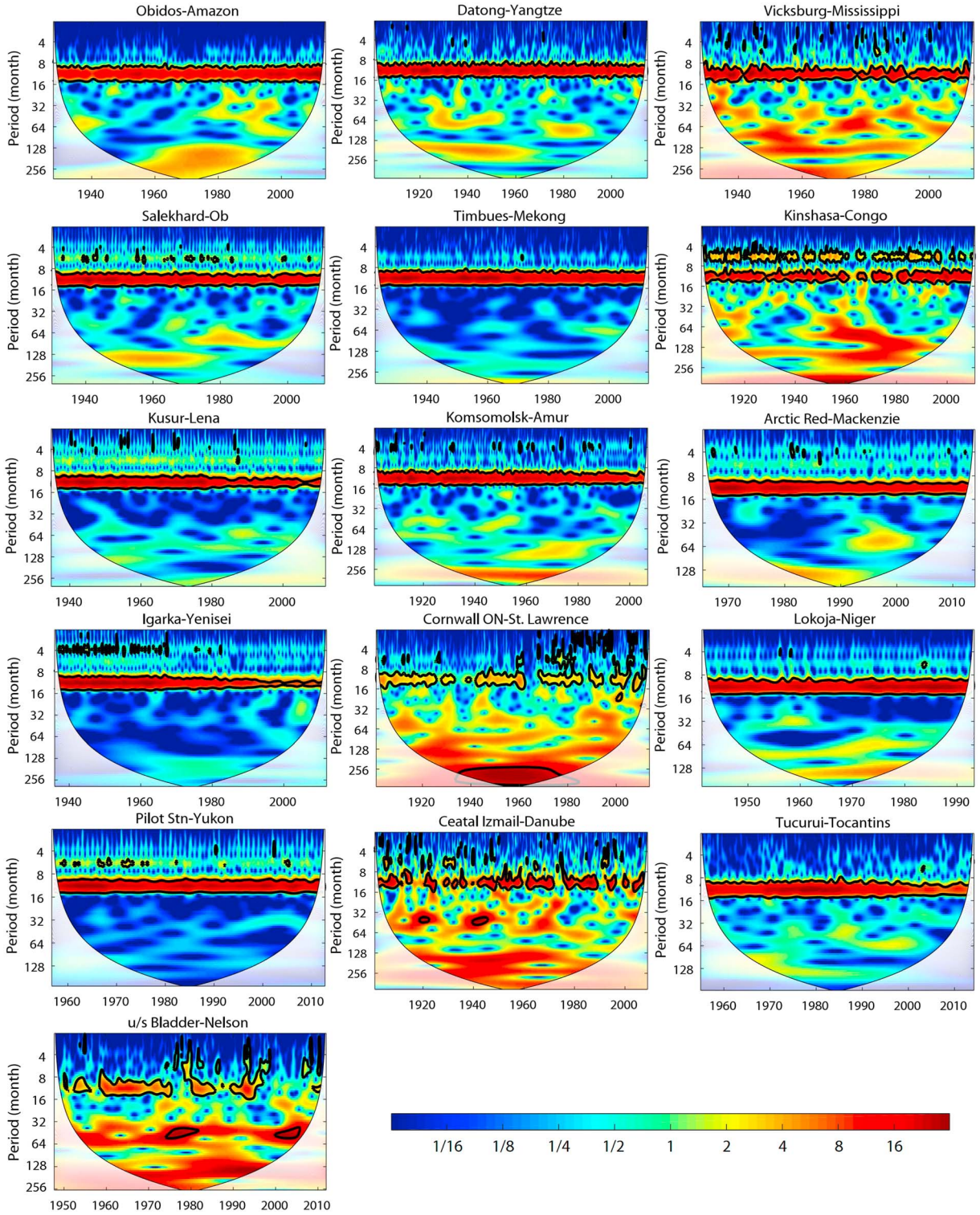

Figure 1. Continuous wavelet transforms for the 16 streamflow series. The period is measured in months. Thick contours denote 5% significance levels against red noise. Pale regions denote the cone of influence where edge effects might distort the results. The color denotes the strength of wavelet power.

thick black contours designate the 5% significance level against red noise, and the pale regions indicate the COI, where edge effects may distort the results. Common features occurred in the streamflow wavelet patterns. Significant annual oscillations (around 12 months) were found in all streamflow series over the

Table 2
Mean Wavelet Transform Coherence Between Streamflow and Individual Predicting Factors

River	AO	Niño3.4	PDO	DMI	NAO	SOI	PET	PRE	WET	TMP
Amazon	0.799	0.802	0.806	0.803	0.773	0.816	**0.895**	0.880	0.890	0.868
Yangtze	0.791	0.782	0.777	0.772	0.788	0.772	0.860	**0.896**	0.874	0.893
Mississippi	0.791	0.792	0.811	0.813	0.772	0.789	0.843	**0.852**	0.837	0.852
Ob	0.785	0.783	0.794	0.774	0.775	0.779	0.879	0.874	0.836	**0.920**
Mekong	0.775	0.811	0.789	0.782	0.806	0.785	0.892	0.889	**0.903**	0.901
Congo	0.790	0.783	0.787	0.785	0.794	0.785	0.846	**0.871**	0.862	0.868
Lena	0.790	0.782	0.781	0.784	0.782	0.793	0.904	0.897	0.862	**0.939**
Amur	0.782	0.776	0.778	0.813	0.786	0.781	0.867	0.884	0.875	**0.902**
Mackenzie	0.768	0.773	0.782	0.772	0.774	0.804	0.902	0.868	0.859	**0.927**
Yenisei	0.775	0.775	0.785	0.795	0.777	0.793	0.891	0.888	0.864	**0.944**
St. Lawrence	0.802	0.786	0.796	0.795	0.776	0.776	0.835	0.819	0.795	**0.843**
Niger	0.778	0.773	0.795	0.781	0.775	0.759	0.894	0.895	0.900	**0.904**
Yukon	0.812	0.772	0.803	0.761	0.757	0.775	0.902	0.857	0.865	**0.935**
Danube	0.790	0.774	0.780	0.776	0.778	0.787	0.829	**0.900**	0.867	0.833
Tocantins	0.781	0.804	0.793	0.780	0.776	0.797	**0.886**	0.878	0.876	0.831
Nelson	0.797	0.783	0.801	0.766	0.781	0.778	**0.838**	0.837	0.829	0.831

Note. Values are the mean wavelet coherence at significant locations across all scales and times.
Entries in bold indicate the factor with the highest coherence. Entries underlined indicate the ocean signal with the highest coherence. AO = Arctic Oscillation; PDO = Pacific Decadal Oscillation; DMI = Dipole Mode Index; NAO = North Atlantic Oscillation; SOI = Southern Oscillation Index; PET = potential evapotranspiration; PRE = total precipitation; WET = number of rainy days; TMP = mean temperature.

study period. Although many rivers showed a continuous annual periodicity, other rivers displayed intermittent breaks. The Mississippi and the Yenisei rivers showed a slight discontinuity in annual periodicity, whereas the Congo, St. Lawrence, Danube, and Nelson rivers showed more frequent breaks in annual periodicity. Some scattered significant periodicities were also revealed. Periodicities of around 4 to 6 months were found for the Yangtze, Mississippi, Ob, Congo, Lena, Amur, Mackenzie, Yenisei, St. Lawrence, Yukon, Danube, and Nelson rivers. A strong periodicity of approximately 20–32 years was also observed for the St. Lawrence river from the 1930s to the 1980s. The CWT also revealed a 3- to 4-year oscillation in the Danube river during the 1920s and 1940s and in the Nelson river during the 1970s and 2000s.

4.2. Individual Factors Controlling Streamflow Variability

The effects of individual factors on variations in streamflow are summarized in Tables 2 and 3. To highlight the most important variables for each river, the factor with the highest coherence is shown in bold, and the ocean signal with the highest coherence is underlined. The mean coherence value at significant domains for all rivers surpassed 0.8, which demonstrated high covariability between streamflows and meteorological factors/ocean signals (Table 2). TMP was the dominant meteorological factor for many of the rivers: It was the meteorological factor with the highest coherence for eight streamflow series. PRE and PET were next in importance, with the highest coherence for four and three streamflow series, respectively. Ocean signals generally had less coherence with streamflow than the meteorological factors. Among the six ocean signals we studied, the PDO and the AO were the most common influencing signals, both accounting for the highest variation coherence for five rivers.

Looking at the PASC (Table 3), meteorological factors make greater contributions than ocean signals to the variation in streamflow in rivers. PRE was the dominant meteorological factor with the greatest value for 11 rivers. WET and PET were the dominant factors for three and two rivers, respectively. The highest PASC for meteorological factors ranged from 30.1% to 69.4% across all rivers, with an average largest PASC of 51.5%. When we considered the best individual factors to explain streamflow variations, PRE stood out since it was in the top two for all 16 rivers. PRE was followed by WET (10 rivers) and PET (six rivers) and lastly TMP (zero rivers). Ocean signals generally had lower PASC values than meteorological factors. Among the six ocean signals, PDO was the most dominant, accounting for the highest PASC for eight rivers. Next in importance were Niño 3.4 and the NAO, which both had for the highest PASC for three rivers. The DMI and the AO was the dominant signal for one river. The highest PASC for ocean signals ranged from 5.1% to 15.1% across all rivers, with an average largest PASC of 9.3%.

Table 3
PASC (%) for the Wavelet Transform Coherence Between Streamflow and Individual Factors

River	AO	Niño3.4	PDO	DMI	NAO	SOI	PET	PRE	WET	TMP
Amazon	7.47	15.08	10.91	8.98	5.48	13.79	32.61	42.98	**47.51**	26.26
Yangtze	7.25	5.98	9.78	3.97	6.02	3.46	42.34	**69.39**	48.38	23.67
Mississippi	5.27	4.50	8.84	5.27	5.87	4.10	34.16	**55.76**	48.49	24.33
Ob	5.08	3.72	4.65	5.12	4.57	3.93	52.47	**54.58**	48.53	21.86
Mekong	3.91	7.35	9.28	6.35	6.91	4.42	28.06	**40.74**	29.40	27.81
Congo	7.24	7.61	5.51	4.69	9.75	6.59	27.03	**46.47**	35.59	23.01
Lena	7.18	3.86	9.24	6.23	6.00	4.22	40.76	**62.31**	35.59	21.27
Amur	6.24	3.70	6.28	6.86	7.59	2.66	37.41	**66.14**	44.90	22.15
Mackenzie	4.39	7.44	7.59	4.09	6.71	8.68	43.55	**48.38**	43.12	25.30
Yenisei	4.50	8.11	5.32	5.82	3.69	9.02	**42.01**	40.38	23.23	20.41
St. Lawrence	6.62	8.80	8.92	7.01	7.41	8.23	25.79	**34.54**	17.31	19.34
Niger	6.33	5.52	7.26	7.13	5.11	2.39	41.04	**61.97**	60.09	36.46
Yukon	7.48	6.44	10.68	3.51	3.73	4.94	40.98	50.31	**51.63**	23.35
Danube	11.29	6.83	6.61	5.57	7.22	5.46	29.34	57.01	**57.03**	19.56
Tocantins	6.09	11.83	7.24	3.57	3.84	8.99	25.58	**55.24**	31.29	21.69
Nelson	5.01	4.44	3.21	6.87	7.90	5.70	**30.11**	27.89	18.93	18.11

Note. PASC refers to the percent area of significant coherence relative to the whole wavelet scale-time domain at all locations at various scales (outside the cone of influence). Entries in bold indicate the factor with the highest PASC. Entries underlined indicate the ocean signal with the highest PASC. AO = Arctic Oscillation; PDO = Pacific Decadal Oscillation; DMI = Dipole Mode Index; NAO = North Atlantic Oscillation; SOI = Southern Oscillation Index; PET = potential evapotranspiration; PRE = total precipitation; WET = number of rainy days; TMP = mean temperature.

Figure 2 depict the WTC results for streamflow and the single factor (all proved to be meteorological factors) that best explains streamflow variations in each river. The strong coherence (red areas) and high PASC (areas bounded by thick contours) are clear. Significant annual covariance prevailed during the entire study period for 12 of the rivers (the Amazon, Yangtze, Ob, Mekong, Congo, Lena, Amur, Mackenzie, Yenisei, Niger, Yukon, and Tocantins rivers). Among these, the Ob, Congo, Lena, Amur, Mackenzie, Yenisei, and Yukon rivers had in-phase (positive) correlations with their predicting factors. WET led the Amazon river streamflow by about 90°, which means that streamflow lagged behind WET by around 3 months during the entire study period. PRE led the Yangtze, Mekong, Niger, and Tocantins rivers by about 45° (approximately 1.5 months). For the Mississippi, St. Lawrence, Danube, and Nelson rivers, intermittent annual oscillations were detected with complicated phase relationships. Strong semiannual oscillations were observed in the WTC results for the Congo and Niger rivers, with PRE leading streamflow by about 90° (1.5 months), and for the Yenisei river, with PET leading streamflow by about 315° (5.25 months).

Significant interannual covariance occurred in all rivers with varying phase differences. For most rivers, meteorological factors either led streamflow series by about 45° (4–16 months) or were in-phase at the interannual level. The Yangtze, Mississippi, Ob, Lena, Amur, Danube, and Tocantins rivers had very high PASC for interannual covariance. Decadal periodicity existed for almost all rivers, except the Mekong, Congo, Mackenzie, and Tocantins rivers, where the PASC for decadal covariance was small. The decadal relationships between streamflow and factors were generally in-phase. However, PRE led streamflow in the Ob, Congo, and St. Lawrence rivers by about 45° (1–2 years), Yenisei river streamflow and PET were in antiphase (about 5 years), and PET led the Nelson river streamflow by about 315° (about 9.5 years). Interdecadal oscillations were detected in the Amazon, Mississippi, Amur, St. Lawrence, and Danube rivers. All interdecadal oscillations showed approximately in-phase relationships between streamflow and their single factor.

Figure 3 shows the WTC results for streamflow in individual rivers and the single ocean signal that best explains streamflow variations in each river. Scattered annual periodicities with complicated phase relationships were found for all rivers during the study period. Interannual oscillations (mainly 2–5 years) with an almost antiphase relationship between streamflow and PDO were observed for the Yangtze, Mississippi, and Yukon rivers during the first half of the twentieth century. Similar interannual oscillations between streamflow and PDO were seen in the Mekong, Lena, Mackenzie, St. Lawrence, and Niger rivers in the second half of the twentieth century. Interannual oscillations between streamflow and Niño 3.4 were found for the Amazon, Yenisei, and Tocantins rivers, with Niño 3.4 leading streamflow by about 315° (1.5–4.5 years) during the second half of the twentieth century. The Ob river and the DMI showed scattered interannual

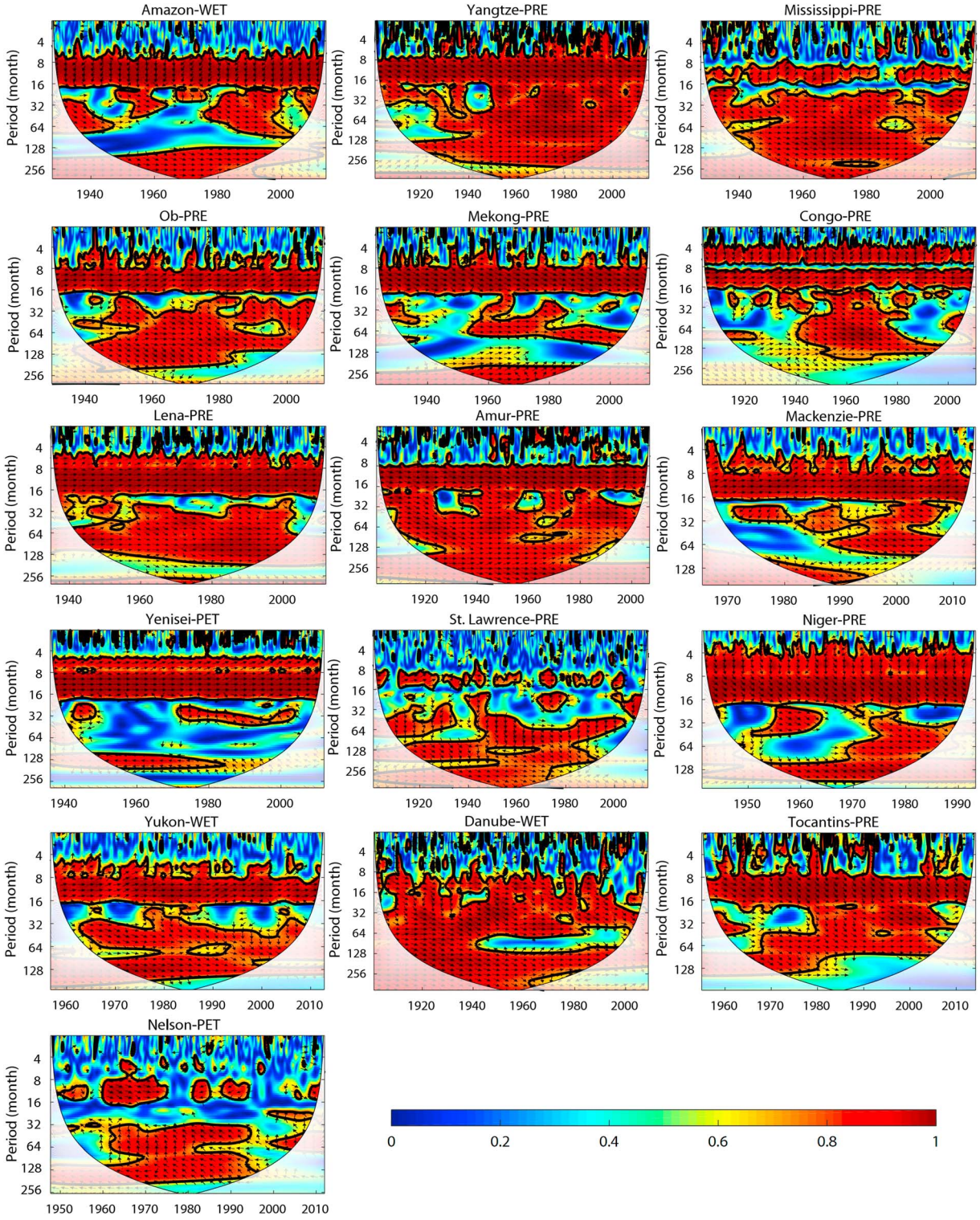

Figure 2. Wavelet transform coherence between streamflow series and meteorological factors. The period is measured in months. Each subplot shows the wavelet transform coherence between streamflow in a single river and the individual meteorological factor that best explains streamflow variation in that river. Thick contours denote 5% significance levels against red noise. Pale regions denote the cone of influence where edge effects might distort the results. Small arrows denote the relative phase relationship (in-phase, arrows point right; antiphase, arrows point left). The color denotes the strength of coherence. WET = number of rainy days; PRE = total precipitation; PET = potential evapotranspiration.

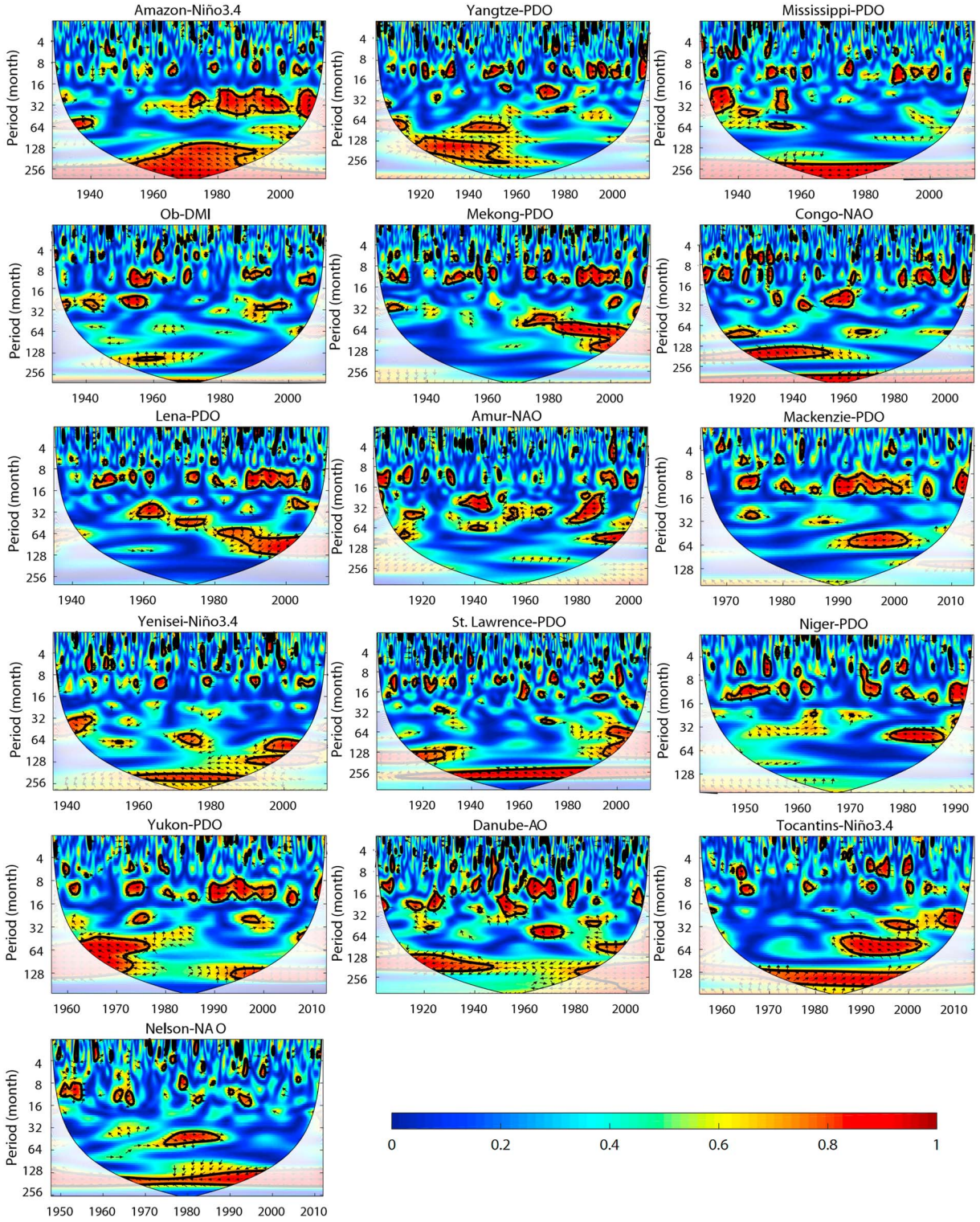

Figure 3. Wavelet transform coherence between streamflow series and ocean signals. The period is measured in months. Each subplot shows the wavelet transform coherence between streamflow in a single river and the individual ocean signal that best explains streamflow variation in that river. Thick contours denote 5% significance levels against red noise. Pale regions denote the cone of influence where edge effects might distort the results. Small arrows denote the relative phase relationship (in-phase, arrows point right; antiphase, arrows point left). The color denotes the strength of coherence. AO = Arctic Oscillation; PDO = Pacific Decadal Oscillation; NAO = North Atlantic Oscillation; DMI = Dipole Mode Index.

Table 4
Coherence Between Streamflow and Multiple Meteorological Factors

River	Single factor	WTC	PASC(%)	Two factors	MWC	PASC(%)	Three factors	MWC	PASC(%)
Amazon	WET	0.89	47.51	WET-PET	0.94	**48.31**	WET-PRE-PET	0.98	43.03
Yangtze	PRE	0.9	**69.39**	PRE-PET	0.96	67.25	PRE –TMP –PET	0.98	64.8
Mississippi	PRE	0.85	55.76	PRE-TMP	0.94	**58.54**	PRE –TMP –PET	0.97	56.23
Ob	PRE	0.87	54.58	PRE-PET	0.94	**58.45**	PRE-TMP-PET	0.97	54.86
Mekong	PRE	0.89	40.74	PRE-PET	0.95	**43.44**	WET-PRE-PET	0.97	42.68
Congo	PRE	0.87	46.47	WET-PRE	0.95	47.76	WET-PRE-PET	0.98	**48.79**
Lena	PRE	0.9	**62.31**	PRE-PET	0.95	58.49	WET-PRE-PET	0.97	54.4
Amur	PRE	0.88	66.14	PRE-PET	0.95	**67.24**	PRE-TMP-PET	0.98	63.42
Mackenzie	PRE	0.87	48.38	PRE-PET	0.95	50.13	WET-PRE-PET	0.98	**52.25**
Yenisei	PET	0.89	42.01	PRE-PET	0.95	**45.31**	WET-PRE-PET	0.97	44.13
St. Lawrence	PRE	0.82	34.54	PRE-PET	0.93	39.48	PRE-TMP-PET	0.98	**43.11**
Niger	PRE	0.9	**61.97**	WET-PRE	0.96	60.59	WET-PRE-PET	0.98	57.64
Yukon	WET	0.87	51.63	WET-PET	0.95	**52.73**	WET-PRE-PET	0.98	52.12
Danube	WET	0.87	57.03	PRE-TMP	0.96	68.58	PRE-TMP-PET	0.97	**70.15**
Tocantins	PRE	0.88	**55.24**	PRE-PET	0.94	53.89	WET-PRE-PET	0.97	48.16
Nelson	PET	0.84	30.11	PRE-PET	0.93	**30.79**	WET-TMP-PET	0.97	27.37

Note. Entries in bold indicate the factor with the highest PASC for streamflow variations for each river. WTC = wavelet transform coherence; PASC = percent area of significant coherence; MWC = multiple-wavelet coherence; PRE = total precipitation; WET = number of rainy days; PET = potential evapotranspiration; TMP = mean temperature.

periodicities in the 1940s, 1960s, and 1990s with complicated phase angles. Scattered interannual oscillations with the NAO existed for the Congo river mainly during the 1940s and 1960s, for the Amur river during the last century, and for the Nelson river in the 1980s, all with complicated phase relationships. The Danube river and the AO had interannual periodicities mainly during the period 1960–1980, also with complicated phases. Decadal periodicity between streamflow and the PDO was observed for the Yangtze river from the 1920s to the 1960s, for the Mekong river in the 1990s, the Lena river in the 1990s, the St. Lawrence river in the 1920s and 1990s, and the Yukon river in the 1970s and 1990s, again, all with complicated phase differences. Almost antiphase decadal periodicity was observed between Niño 3.4 and streamflow in the Amazon river in the 1970s–1980s and in the Yenisei river in the 1960s–1990s and 1990–2000. Niño 3.4 led streamflow in the Tocantins river by about 315° (about 9.5 years) in decadal periodicity during the 1970s to 1990s. NAO led streamflow in the Congo river by about 45° (about 1.25 year) in decadal periodicity during the 1920s to 1950s. Anti-phase decadal oscillations were observed between streamflow in the Nelson river and the NAO between the 1970s and 1990s. Anti-phase bidecadal oscillations were found between streamflow in the Amazon river and Niño 3.4 from the 1950s to the 1980s, between streamflow in the Mississippi river and the PDO from the 1960s to the 1980s, between streamflow in the Congo river and the NAO from the 1950s to the 1960s, and between streamflow in the St. Lawrence river and the PDO from the 1930s to the 1980s.

4.3. Combined Factors Explaining Streamflow Variability

Table 4 summarizes the combinations of meteorological factors that optimally explain streamflow variations (individual-factor, plus two-factor, and three-factor combinations). The average MWC coherence value at significant domains for all two-factor combination cases was 0.94, higher than the average WTC (0.8). Among all the two-factor combinations, PRE and PET were the most common, being the best two-factor combination for explaining streamflow variation for 10 rivers (Table 4). WET and PET, WET and PRE, and PRE and TMP were each the best two-factor combination for two rivers. A comparison between the two-factor cases and individual-factor cases showed that the mean coherence increased for all rivers when two factors were combined. An increase in PASC occurred in 12 rivers (the Amazon, Mississippi, Ob, Mekong, Congo, Amur, Mackenzie, Yenisei, St. Lawrence, Yukon, Danube, and Nelson rivers). Although only the Danube river (11.6% increase) showed an increase that was more than 5% and considered significant, the smaller increases in the PASC in the other rivers also indicate that additional factors result in an increase in the amount of streamflow variation explained. In these 12 rivers, the small increases in PASC with two combined factors (compared to the WTC) were due to oscillations with periodicity around

4–8 months (Figures 3 and 4). The combination of two factors explained a greater amount of streamflow variation at this periodicity than any single factor, and the additional factor was not correlated with the previous single factor at oscillations around 4–8 months.

The significant increase in PASC in the Danube river with two factors (compared to the WTC) was due to oscillations with periodicity around 5 years. Both PRE and TMP explained a certain amount of streamflow variation, and they were not correlated at oscillations around this periodicity (Figure 4). Another six rivers showed a decrease in PASC with two factors, which may be attributed to the simultaneously increased threshold for statistical significance threshold when an additional factor is added (Ng & Chan, 2012). Furthermore, most areas with significant correlation between streamflow and the additional factor were located within the area that already showed significant coherence for the best individual factor.

Table 5 and Figure 5 summarize the combinations of meteorological factors and ocean signals that optimally explain streamflow variations. Among all the combinations, PRE formed the most common optimal combination with ocean signals for explaining variations in streamflow. However, the PASC increased with an additional factor only for the Mekong river (an increase of 1.57% after adding Niño 3.4 compared with PRE alone). Similar to above, part of the reason for the lack of PASC expansion was that most areas with significant correlation between streamflow and the additional ocean signals were located within the area that already showed significant coherence for the best individual meteorological factor.

Likewise, when there were three predictor variables in the MWC analysis, all coherences further increased to nearly 1 (Table 4 and Figure 6). However, the PASC decreased for 12 rivers. Only the Congo, Mackenzie, St. Lawrence, and Danube rivers showed increases in the PASC when taking three predictor variables, and none of these increases was statistically significant (Table 4). The main reason for the disagreement in the changes of coherence and PASC results was that the additional variance explained by a third factor at a particular periodicity and time was already accounted for by the first two factors. The contribution from some factors was weakened by overlapping effects because of the collinearity among factors. Therefore, only an additional factor that can independently explain a fair amount of additional streamflow variability would make a significant contribution (Hu et al., 2017). Furthermore, as described above, the PASC threshold for statistical significance increases when additional factors are added (Ng & Chan, 2012). The increased PASCs for the Congo, Mackenzie, St. Lawrence, and Danube rivers (as compared to the PASCs with two predictors) were due to oscillations with periodicities around 4–8 months (Figures 4 and 6). For these rivers, the combination of three factors explained a fair amount of streamflow variation, and the third additional factor was not correlated with the previous two factors at oscillations with periodicities of 4–8 months.

To summarize, we conducted a comparison of the coherence between streamflow and one factor, two factors, or three factors for 16 of the large rivers in the world: The optimal predictor(s) for each river are highlighted in bold in Table 4.

5. Discussion

Only an additional factor that can independently account for a significant amount of streamflow variability will contribute significantly to explaining variations in streamflow (Hu et al., 2017). The variance that is explained by additional factors at any particular periodicity and time may be already accounted for by the existing factors. In our study, the contribution of additional factors may be weakened by overlapping effects because of collinearity among the previous and additional factors. Therefore, the best predictor(s) of streamflow differed from river to river, varying from an individual factor to a combination of two or three factors.

For a river basin, the runoff can be calculated as

$$R = PRE - ET - storage, \tag{7}$$

where R is total runoff (including surface runoff and subsurface drainage), PRE is precipitation, ET is evapotranspiration, and storage represents temporary reservoirs of water such as snow stored at the surface or soil moisture within the soil column (Twine et al., 2004). Storage is negligible at the annual time scale;

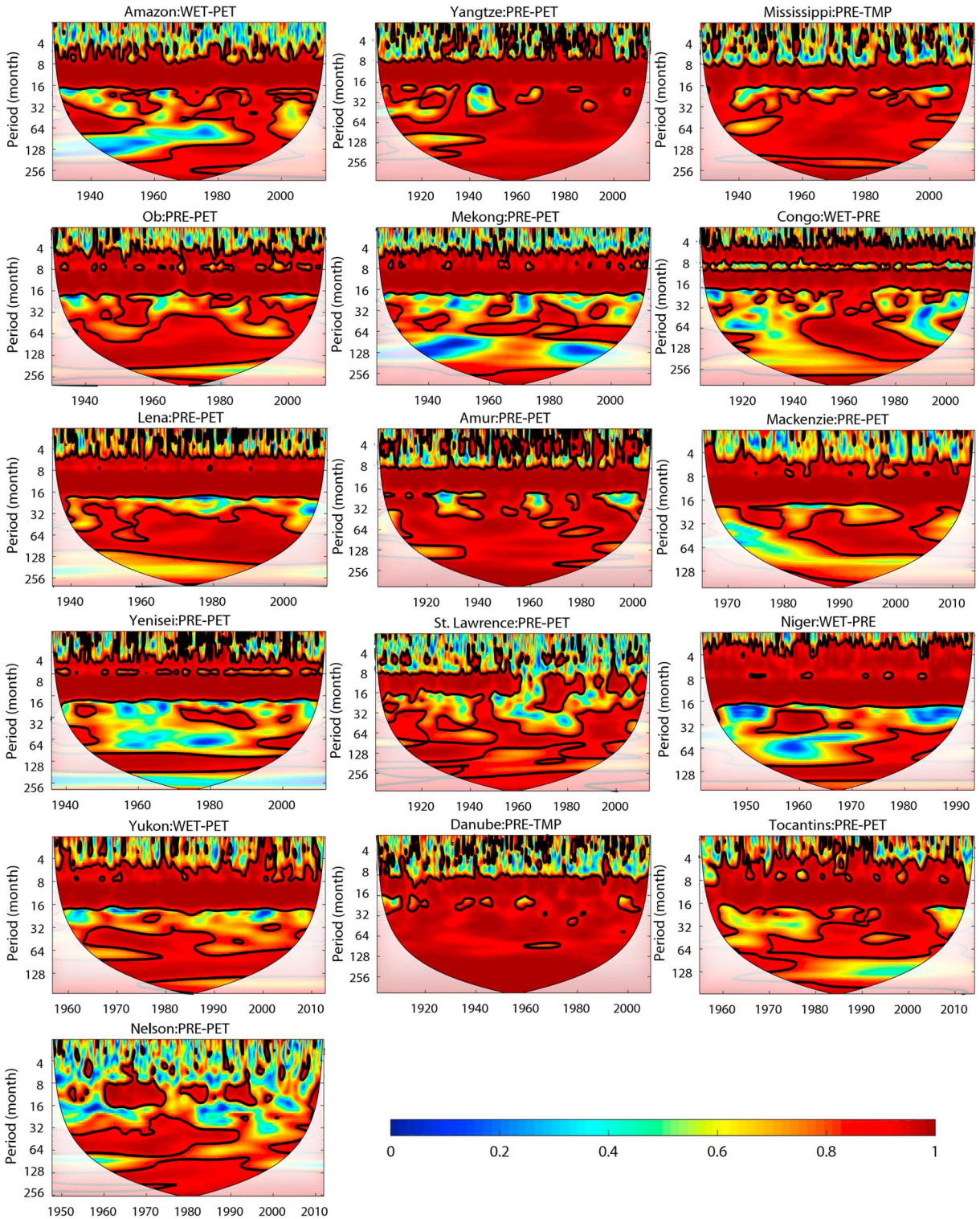

Figure 4. Two-factor multiple wavelet coherence. The period is measured in months. Each subplot shows the multiple wavelet coherence between streamflow in a single river and the best combination of two factors. Thick contours denote 5% significance levels against red noise. Pale regions denote the cone of influence where edge effects might distort the results. The color denotes the strength of coherence. WET = number of rainy days; PRE = total precipitation; PET = potential evapotranspiration; TMP = mean temperature.

Table 5
Coherence Between Streamflow and Meteorological Factor-Ocean Signal Combinations

River	Combined factors	MWC	PASC (%)
Amazon	WET-Niño3.4	0.95	43.83
Yangtze	PRE-AO	0.95	64.67
Mississippi	PRE-PDO	0.94	50.43
Ob	PRE-Niño3.4	0.94	49.18
Mekong	PRE- Niño3.4	0.95	42.31
Congo	PRE-NAO	0.94	42.36
Lena	PRE-NAO	0.95	55.83
Amur	PRE-NAO	0.94	60.55
Mackenzie	PRE-PDO	0.94	42.5
Yenisei	PET-AO	0.95	38.14
St. Lawrence	PRE-PDO	0.92	32.18
Niger	WET-AO	0.95	57.45
Yukon	WET-PDO	0.94	45.08
Danube	PRE-AO	0.95	56.4
Tocantins	PRE-AO	0.94	49.74
Nelson	PRE-Niño3.4	0.93	29.32

Note. PASC = percent area of significant coherence; MWC = multiple-wavelet coherence; WET = number of rainy days; PRE = total precipitation; AO = Arctic Oscillation; PDO = Pacific Decadal Oscillation; NAO = North Atlantic Oscillation; PET = potential evapotranspiration.

thus, runoff is closely correlated with PRE and ET. ET is closely correlated with PET. It is therefore not surprising that PET and PRE or/and WET were the best predictors of streamflow variation for many rivers.

At low latitudes, strong radiative forcing results in high PET, which can have a big impact on streamflow. The WET-PET combination was the best predictor of streamflow variation for the Amazon river. However, areas with significant correlation between streamflow and other factors may have been contained within areas where streamflow and WET-PET had significant coherence. Marengo (2009) detected multidecadal time-scale variations in rainfall and river flow time series in the period 1929–1998, including the relatively wet period from the late 1950s to the mid-1970s in the northern Amazon. Previous studies on the Amazon river have mainly focused on PRE rather than WET. Our results showed that Amazon streamflow was more correlated with WET than PRE. According to Van der Ent et al. (2010), the Río de la Plata basin depends on evaporation from the Amazon forest for 70% of its water resources. Their estimate of the fraction of evaporated water that is recycled within the same Amazon region was 48%. It therefore makes sense that WET-PET was the best predictor of streamflow variation for the Amazon river in our study (Figure 4). Many previous papers have studied the relationships between Amazon streamflow and ocean signals such as the ENSO, PDO, AO, NAO, and the Atlantic multidecadal oscillation (AMO; Marengo, 2009; Marengo et al., 2011; Davidson et al., 2012; Gloor et al., 2013; Espinoza et al., 2014). Our results showed that the ENSO was the dominant ocean signal involved in variations in Amazon streamflow. The interannual coherence revealed in the WTC between Amazon streamflow and Niño3.4 (Figure 3) can be attributed to the fact that interannual rainfall variability in the Amazon basin partially depends on the ENSO. In particular, below-normal rainfall has been recorded in the north and northeast of the Amazon basin during El Niño events (warm ENSO phases), whereas excess rainfall has been recorded during La Niña events (cold ENSO phases). This pattern results in high flood levels for the Amazon river during La Niña events and low flood levels during El Niño events. (Davidson et al., 2012; Espinoza Villar et al., 2009; Sombroek, 2001). In our study, WET combined with Niño 3.4 was the best combination of meteorological factor and ocean signal for the Amazon river (Figure 5). When the ENSO effect was superimposed over a 28-year cycle of variation in precipitation, severe floods and droughts became prevalent (Davidson et al., 2012). The biggest floods occurred when the La Niña phase coincided with the wet phase in the 28-year cycle, which occurred in the mid-1970s. The worst droughts occurred when the El Niño phase coincided with the dry phase of the longer-term cycle, for example, during the 1992 drought (Davidson et al., 2012).

Precipitation was the best predictor for the Tocantins river, and additional factors did not increase the area of coherence. Monthly precipitation has a high level of agreement with river discharge ($R = 0.84$) at a 1-month time lag (Coe et al., 2011). Costa et al. (2003) also showed that about half of the increment in discharge can be explained by an increase in precipitation. Our results suggested Niño3.4 and AO combined with PRE were the best combinations of meteorological factor and ocean signal for explaining variation in streamflow in the Tocantins river. According to Foley et al. (2002), the Tocantins river was drier and warmer than normal during El Niño phases and wetter and cooler during La Niña phases. Little research has focused on the AO and streamflow in the Tocantins river. Our results may provide a new avenue for future study.

PRE-TMP was the best combination of predictors for streamflow in the Mississippi river. It has previously been reported that increased regional precipitation is the dominant driver of positive runoff trends in the upper Mississippi river basin (Frans et al., 2013). Similarly, increased precipitation has led to an upward trend in streamflow in the Mississippi river basin since the 1940s (Zhang & Schilling, 2006). Temperature can affect both evapotranspiration and snowmelt: Both contribute to changes in soil water and thus regulate streamflow (Lu et al., 2010). The PDO was the ocean signal that best explained variation in streamflow in the Mississippi, and PRE-PDO was the best meteorological factor-ocean signal combination. This is consistent with the fact that Mississippi river flow has been reported to be significantly lower during the PDO cold phase than during the PDO warm phase (Tootle et al., 2005; Tootle & Piechota, 2006; Sanchez-Rubio

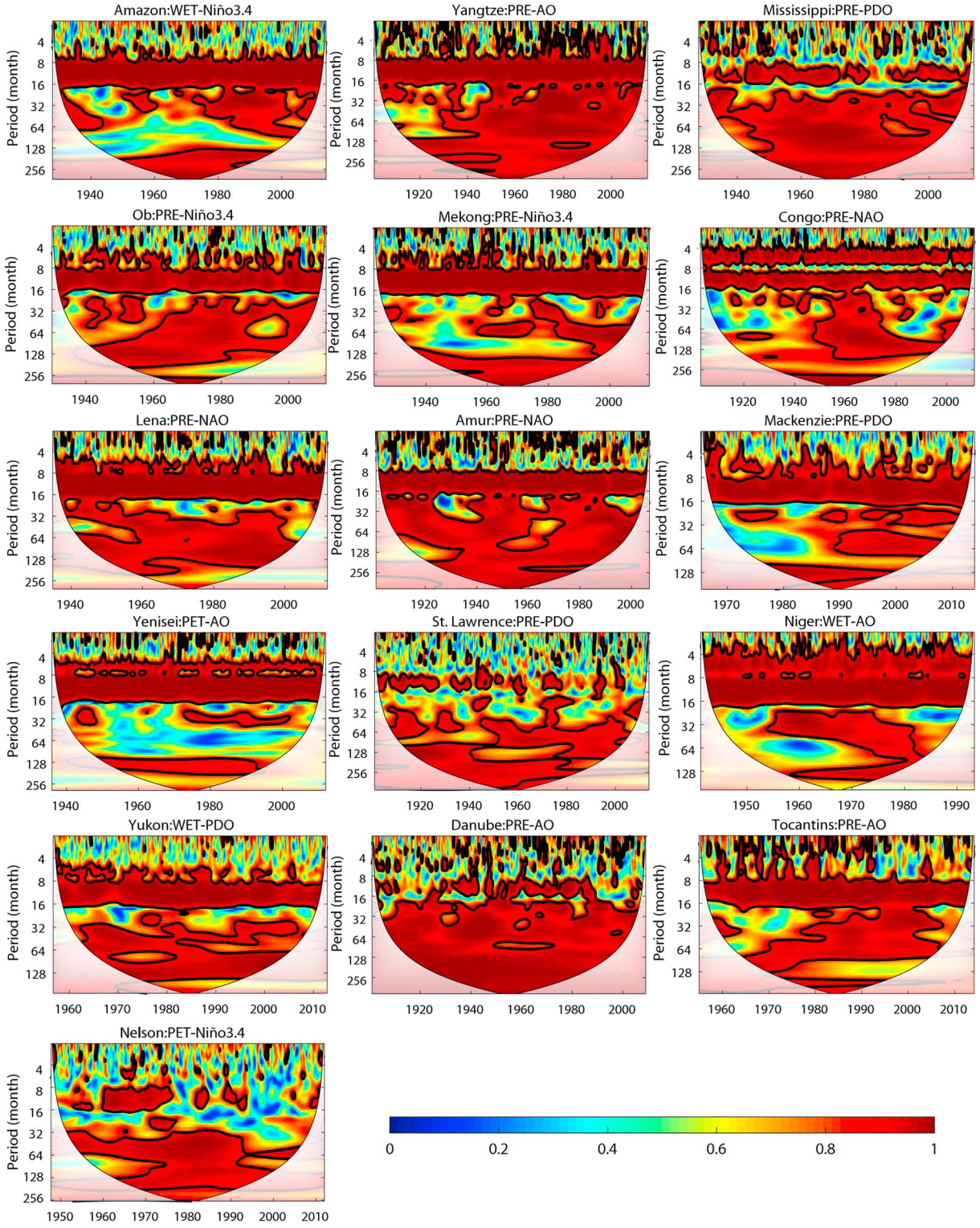

Figure 5. Meteorological factor-ocean signal combination multiple wavelet coherence. The period is measured in months. Each subplot shows the multiple wavelet coherence between streamflow in a single river and the best meteorological factor-ocean signal combination. Thick contours denote 5% significance levels against red noise. Pale regions denote the cone of influence where edge effects might distort the results. The color denotes the strength of coherence. .
WET = number of rainy days; PRE = total precipitation; PET = potential evapotranspiration; AO = Arctic Oscillation; PDO = Pacific Decadal Oscillation; NAO = North Atlantic Oscillation.

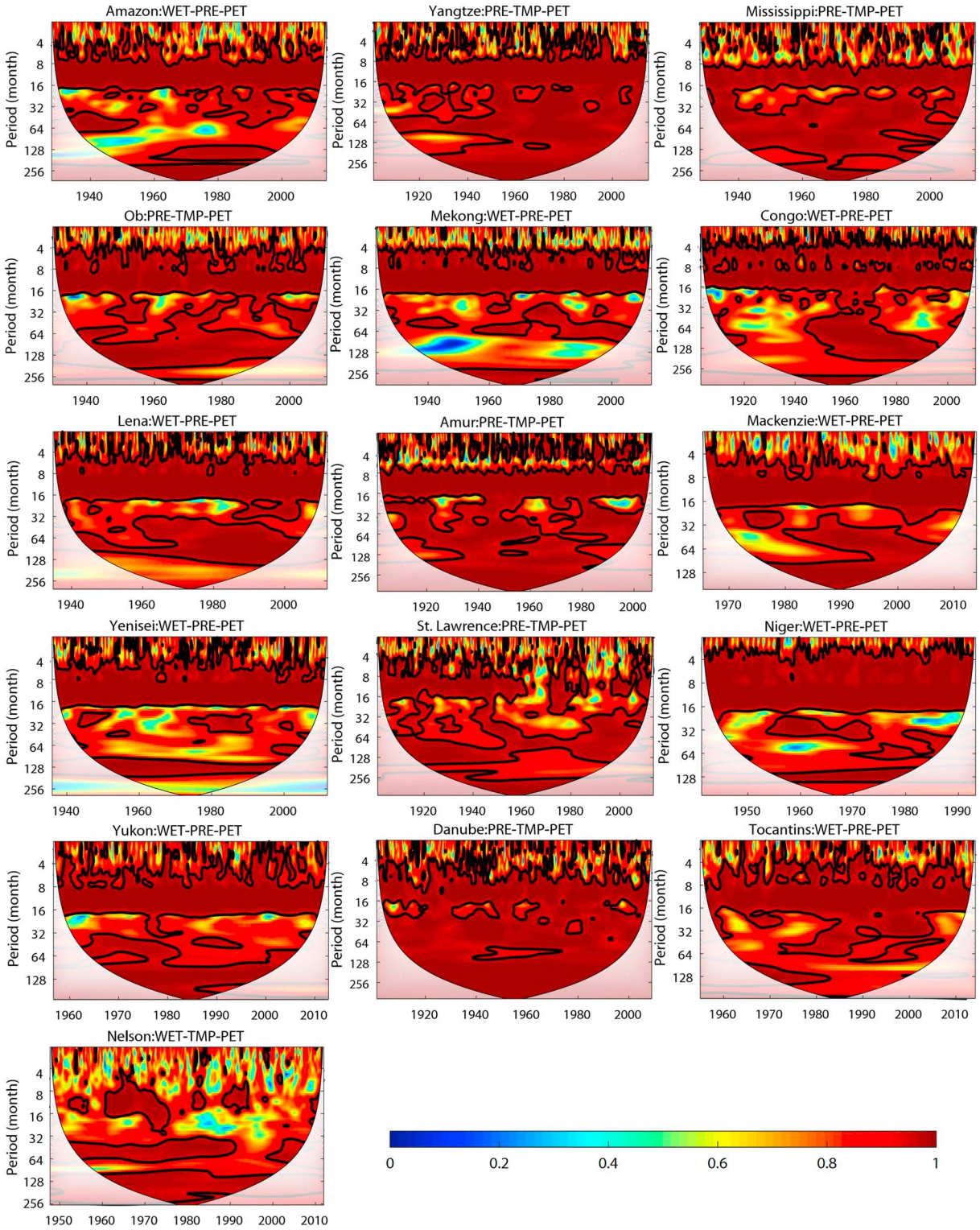

Figure 6. Three-factor multiple wavelet coherence. The period is measured in months. Each subplot shows the multiple wavelet coherence between streamflow in a single river and the best combination of three factors. Thick contours denote 5% significance levels against red noise. Pale regions denote the cone of influence where edge effects might distort the results. The color denotes the strength of coherence. WET = number of rainy days; PRE = total precipitation; PET = potential evapotranspiration; TMP = mean temperature.

et al., 2011; Mallakpour & Villarini, 2016). In addition, long-term Mississippi river flow variability is primarily associated with the interdecadal PDO (Sanchez-Rubio et al., 2011).

PRE-PET was the best predictor for the Mekong river. Much of the streamflow variability in the Mekong river basin results from the monsoonal precipitation regime and terrain topography. There are pronounced relationships between streamflow and annual and wet-season precipitation, especially for the upstream region of the Lancang-Mekong river, for which the percent variance explained was more than 65% in both cases (Fan & He, 2015). Although streamflow variability in the dry season is dominated by snowmelt, a significant portion is explained by soil moisture, and soil moisture dynamics are controlled by evapotranspiration via water extraction by deep roots (mostly in forested areas; Costa-Cabral et al., 2008). In our study, the PDO and Niño3.4 combined with PRE explained more than 40% of streamflow variation for the Mekong river. Delgado et al. (2012) reported a relationship between the variance of the Western North-Pacific monsoon index and PDO intensity that has important implications for hazardous floods in the Mekong area. The ENSO also has a large effect on Mekong river streamflow: Precipitation and discharge decreased, the annual flood period was shorter during El Niño phases, and the opposite occurred during La Niña phases (Räsänen & Kummu, 2013).

WET-PRE-PET was the best predictor for the Congo river. In regions similar to the Congo river, the higher availability of soil moisture under global warming conditions enhances the moisture-evapotranspiration-precipitation loop (Saeed et al., 2013), which in turn greatly impacts streamflow. After anomalously rainy seasons in early 2003 and 2005, about 60–70% of precipitation went to streamflow and evapotranspiration in the Cong basin (Crowley et al., 2006). Our results indicate that PRE-PET alone was not enough to account for the variations in streamflow and that adding WET contributes to the amount explained. Our results suggest that NAO is the ocean signal with the most influence on variations in Congo river streamflow. This is supported by Todd and Washington (2004) who found a strong negative association between the NAO and Congo river discharge during the boreal winter/spring period at both interannual and multiannual time scales. Despite its equatorial location, streamflow in the Congo river in boreal winter/spring appeared more sensitive to influences from the North Atlantic than from the ENSO.

PRE was the best predictor for the Niger river. This is supported by Aich et al. (2014), who found that streamflow in the Niger river was highly sensitive to changes in PRE: A 25% increase in annual precipitation resulted in a 90% increase in modeled discharge, whereas a similar reduction in precipitation caused the annual discharge to decrease by almost 50%. Furthermore, a correlation analysis by Murray et al. (2012) revealed that streamflow changes in the Niger river are tightly linked to changes in rainfall (Pearson correlation coefficient $R = 0.53$). Applying a similar analysis, Roudier and Ducharne (2014) found a similar correlation between rainfall and streamflow for the Niger river ($R = 0.49$) and a smaller correlation between streamflow and changes in PET.

PRE was the best predictor for the Yangtze river. Previous analysis has indicated that runoff trends for the Yangtze river respond closely to precipitation trends (Zhang et al., 2005). Precipitation was significantly correlated with discharge, explaining 80% of the variance in a multiple correlation analysis (Chen et al., 2014). S. L. Yang et al. (2010) found common interannual, decadal, and multidecadal intervals between discharge and precipitation in the Yangtze river, consistent with our results. Our WTC analysis of the relationships between streamflow and ocean signals revealed that the PDO was the ocean signal that best explained variations in Yangtze streamflow. According to X. Zhang et al. (2014), the positive phase of the PDO could lead to reduced precipitation, consequently affecting the long-term water discharge of the Yangtze river. Furthermore, water discharge from the Yangtze river consists of cycles that are closely related to the typical PDO cycles (i.e., 15- to 20-year cycles, on average; Zhang et al., 1997). However, a combination of PRE-AO was the best predictor for the Yangtze river among the meteorological factor-ocean signal combinations, which may be attributed to the strong correlation between the AO and summer rainfall in the region. According to Gong et al. (2002), summer rainfall along the Yangtze river was strongly correlated with the May AO, with a correlation coefficient of −0.39, significant above the 99% confidence level. Rainfall over the Yangtze river decreased by about 3–9% with a strengthening of the May AO index by one standard deviation.

PRE-TMP-PET was the best predictor for the Danube river. The source of the Danube is in the Alps, and the portions of the Danube streamflow originating from icemelt, snowmelt, and rain varied from approximately

33% each in the upstream section to about 2%, 75%, and 25%, respectively, in the downstream section. Since temperature decreases with increasing altitude, large amounts of precipitation fell in the form of snow at higher elevations, and release from this temporary storage is strongly temperature dependent. Furthermore, the lower temperatures and presence of snow at higher elevations weakens evaporation and thus favors higher specific runoff (Weber et al., 2010). This is supported by Szolgayova et al. (2014) who found that the precipitation-discharge wavelet coherence spectrum showed significant coherence for most periods at almost all times with cross-wavelet spectra and wavelet coherence. Previous studies on Danube streamflow and ocean signals mainly focused on the NAO and the ENSO. Our results showed that the AO accounted for a greater part of streamflow variation. This is in agreement with Ionita et al. (2015), who found that the leading mode of dryness/wetness variability was strongly related to the different phases of the AO.

PRE-TMP-PET was the best predictor for the St. Lawrence river. The St. Lawrence river area is characterized by harsh winters, and winter streamflow is mainly derived from aquifers that are recharged in the spring, during snowmelt, and in the fall, when evapotranspiration is subdued. Winter precipitation has a significant impact on spring streamflow, which is mainly fed by snowmelt. Spring streamflow accounts for at least half of the annual streamflow in Quebec rivers, including the St. Lawrence river (Assani & Tardif, 2005). In some catchments throughout Quebec, over 70% of annual infiltration takes place during snowmelt and over 60% of aquifer water turns up as streamflow (Lavigne et al., 2010; Nastev et al., 2005). Thus, the percentage of precipitation falling as either rain or snow directly affects water supplied from the snowpack in the spring and the amplitude and timing of streamflow during the winter and spring (Hodgkins et al., 2003). Our results showed that, individually, PRE, TMP, and PET could not fully account for variations in streamflow in the St. Lawrence river but that the combination of PRE-TMP-PET is the best predictor.

At high latitudes, PET and PRE and/or WET tend to be important. Rivers at high latitudes exhibit PRE maximums in July and minimums in February and March. PRE-WET tends to peak in autumn and be lowest in summer (Serreze et al., 2002). The influence of PRE/WET and PET on streamflow varies for different rivers. Reported measurements of mean streamflow ratio (streamflow/PRE) varied for the major Arctic-flowing rivers. Values for the Ob river ranged from 0.25 to 0.33, considerably lower than values for the Yenisey (0.47 to 0.54), Lena (0.46 to 0.61), Amur (0.38–0.67), and Yukon (0.7) rivers (Carey & Woo, 1999; Serreze et al., 2002; Suzuki et al., 2006). Existing estimates for the Mackenzie river were intermediate (0.30 to 0.46; Bowling et al., 2000). These differences in streamflow ratio might derive from differences in PET for the different rivers, with PET values being especially high for the Ob river. Generally, the streamflow ratio was consistent with the high fraction of annual precipitation and snowmelt lost through evapotranspiration, especially in summer. A clear progression in January temperatures occurred from relatively mild conditions in the Ob (−18.7 °C) to very cold conditions in the Lena (−35.0 °C), fostering stronger summer PET in the Ob river and weaker summer PET in the Lena river. The number of snow-free days was also much greater in the Ob river, pointing to earlier and more prolonged warming of the soil, also contributing to high evapotranspiration rates. Furthermore, a larger part of the Ob and over 6% of the Mackenzie are characterized as wetlands, which contributes to the higher evapotranspiration for these rivers (Serreze et al., 2002). For large domains in northern Eurasia, about 25% of July precipitation was associated with the recycling of water vapor evapotranspirated within each domain (Serreze et al., 2002). Our findings for high-latitude rivers are consistent with the above results. We found that PRE-PET was the best predictor for the Ob, Amur, Yenisei, and Nelson rivers. WET-PET was the best predictor for the Yukon river, indicating that future Yukon streamflow studies may benefit from taking WET rather than PRE into consideration. For the Mackenzie river, WET-PRE-PET was the best predictor. However, PRE was the best predictor for the Lena river because of the low influence of PET for this river.

In summary, due to the multiple-scale characteristics of streamflow and related environmental variables, single factors can fail to capture the salient features of the underlying processes. The best predictors of streamflow differed for different rivers, although all were either individual meteorological factors or combinations of meteorological factors. This may be attributed to the fact that meteorological factors are directly linked to streamflow whereas ocean signals influence streamflow indirectly via hydrologic/meteorological processes. The most common predictors were PRE or/and WET combined with PET. For some rivers, a single factor was sufficient to account for the variations in streamflow, but others required two or three factors in combination. The differences between rivers arise from the discrepancies in their latitudes, radiative forcing, topography, vegetation coverage, hydrological processes, and so forth. Although the combined

meteorological factor/ocean signal case is less efficient than combining two meteorological factors, the former may be favored when information about certain meteorological factors is unavailable. Furthermore, in terms of operational practices for water resources, the predictability of some of the ocean signals may be much higher than the dominant influencing factors (such as WET and PET), despite the ocean signals not being the dominant factor. Therefore, secondary predictors with "good enough" coherence and high predictability may actually be more useful for operational water resource planning that requires predictability several months in advance. Our study has some limitations. We studied globally recognized environmental variables. However, we did not take into account some region-specific variables, such as the AMO. The AMO is related to the multidecadal variability of many regional climates, including the North American and European summer climate (Knight et al., 2006). During AMO warmings, much of the United States experiences lower rainfall than normal; outflow from the Mississippi river varies by 10% between warm and cool AMO phases (Enfield et al., 2001). Also, we did not assess combinations of four or more factors. However, according to our results, there is a high chance that the PASC will decrease as more variables are taken into consideration.

6. Conclusions

Temporal scale-dependent multivariate relationships between streamflow and meteorological factors/ocean signals in 16 of the world's large rivers were identified using WTC and MWC. Prior to the multivariate analysis, the CWT was used to detect temporal patterns in streamflow. The CWT results showed that significant annual oscillations occurred in all streamflow series over the study period, either with continuous annual periodicity or with intermittent breaks. Oscillations with periodicities of around 4 to 6 months were also found in many rivers.

A comparison of the results from the WTC and MWC analyses indicated that streamflow variation could be best explained by one, two, or three meteorological factors. To summarize, WET-PET was the best predictor of variation in streamflow for the Amazon and the Yukon rivers; PRE-PET was the best predictor for the Mekong, Ob, Amur, Yenisei, and Nelson rivers; PRE was the best predictor for the Tocantins, Niger, Yangtze, and Lena rivers; PRE-TMP was the best predictor for the Mississippi river; WET-PRE-PET was the best predictor for the Congo and Mackenzie rivers; PRE-TMP-PET was the best predictor for the Danube and St. Lawrence rivers. The combination of factors that best explained streamflow variations differed among the rivers, although PRE or WET either alone or in combination with other factors was a dominant predictor for all rivers. The most common best predictor was PRE or/and WET combined with PET. The differences in best predictor were due to differences in latitude, radiation forcing, terrain, vegetation coverage, hydrological processes, and so on.

Our results are conducive to a better understanding of the trends in global river streamflow. The results suggest that an efficient and promising way to predict streamflow at different time scales under changing climate scenarios and changing atmospheric and oceanic conditions is to focus on the best predictor. Our conclusions will also be valuable for planning and implementing operational strategies for the sustainable use of available water resources. Limitations of this study include not incorporating more meteorological factors and ocean signals and excluding four-factor combinations. We did not include snow in our wavelet analysis because of the lack of global data for snow depth/coverage/snow water equivalent during our study period. However, the amount of snow is closely related to temperature, so some of the effects of snow may have been accounted for indirectly by taking temperature into consideration. These limitations should be addressed in future studies.

Acknowledgments
This research was supported by the National Natural Science Foundation of China (41622101 and 41877155), the National Key Research and Development Program of China (2016YFC0501604), the Fundamental Research Funds for the Central Universities, and the State Key Laboratory of Earth Surface Processes and Resource Ecology. We are grateful to Dai and Global Runoff Data Centre for providing the global streamflow data (http://www.cgd.ucar.edu/cas/catalog/surface/dai-runoff/index.html), National Oceanic and Atmosphere Administration (NOAA) for providing the climate signals from the oceans (http://www.esrl.noaa.gov/psd/), and Climatic Research Unit for providing the observed climate data (http://www.cru.uea.ac.uk/data/).

References

Aich, V., Liersch, S., Vetter, T., Huang, S., Tecklenburg, J., Hoffmann, P., et al. (2014). Comparing impacts of climate change on streamflow in four large African river basins. *Hydrology and Earth System Sciences*, *18*(4), 1305–1321.

Arnell, N. W. (1999). Climate change and global water resources. *Global Environmental Change*, *9*(S1), S31–S49.

Arnell, N. W., & Gosling, S. N. (2013). The impacts of climate change on river flow regimes at the global scale. *Journal of Hydrology*, *486*, 351–364.

Arnell, N. W., & Lloyd-Hughes, B. (2014). The global-scale impacts of climate change on water resources and flooding under new climate and socio-economic scenarios. *Climatic Change*, *122*, 127–140.

Assani, A., & Tardif, S. (2005). Classification, characterisation et facteurs devariabilité spatial des regimes hydrologiques naturels au Québec (Canada). Approche éco-géographique. *Revue des Sciences de l'Eau1*, *8*, 247–266.

Beck, H. E., De Roo, A., & van Dijk, A. I. (2015). Global maps of streamflow characteristics based on observations from several thousand catchments. *Journal of Hydrometeorology*, *16*(4), 1478–1501.

Bogardi, J. J., Fekete, B. M., & Vörösmarty, C. J. (2013). Planetary boundaries revisited: A view through the 'water lens'. *Current Opinion in Environmental Sustainability*, *5*(6), 581–589.

Bowling, L. C., Lettenmaier, D. P., & Matheussen, B. V. (2000). Matheussen, Hydroclimatology of the Arctic drainage basin. In E. L. Lewis, et al. (Eds.), *The freshwater budget of the Arctic Ocean* (pp. 57–90). Norwell, MA: Kluwer Acad.

Carey, S. K., & Woo, M. K. (1999). Hydrology of two slopes in subarctic Yukon Canada. *Hydrological Processes*, *13*(16), 2549–2562.

Cazelles, B., Chavez, M., Berteaux, D., Ménard, F., Vik, J. O., Jenouvrier, S., & Stenseth, N. C. (2008). Wavelet analysis of ecological time series. *Oecologia*, *156*(2), 287–304.

Chen, J., Wu, X., Finlayson, B. L., Webber, M., Wei, T., Li, M., & Chen, Z. (2014). Variability and trend in the hydrology of the Yangtze River, China: Annual precipitation and runoff. *Journal of Hydrodynamics*, *513*, 403–412.

Chiew, F. H. S., & McMahon, T. A. (2002). Global ENSO-streamflow teleconnection, streamflow forecasting and interannual variability. *Hydrological Sciences Journal*, *47*(3), 505–522.

Coe, M. T., Latrubesse, E. M., Ferreira, M. E., & Amsler, M. L. (2011). The effects of deforestation and climate variability on the streamflow of the Araguaia River, Brazil. *Biogeochemistry*, *105*(1-3), 119–131.

Cook, B. I., Bell, A. R., Anchukaitis, K. J., & Buckley, B. M. (2012). Snow cover and precipitation impacts on dry season streamflow in the Lower Mekong Basin. *Journal of Geophysical Research*, D16116. https://doi.org/10.1029/2012JD017708

Costa, M. H., Botta, A., & Cardille, J. A. (2003). Effects of large-scale changes in land cover on the discharge of the Tocantins River, Southeastern Amazonia. *Journal of Hydrology*, *283*(1-4), 206–217.

Costa-Cabral, M. C., Richey, J. E., Goteti, G., Lettenmaier, D. P., Feldkötter, C., & Snidvongs, A. (2008). Landscape structure and use, climate, and water movement in the Mekong River basin. *Hydrological Processes*, *22*(12), 1731–1746.

Crowley, J. W., Mitrovica, J. X., Bailey, R. C., Tamisiea, M. E., & Davis, J. L. (2006). Land water storage within the Congo Basin inferred from GRACE satellite gravity data. *Geophysical Research Letters*, *33*, L19402. https://doi.org/10.1029/2006GL027070

Dai, A. (2016). Historical and future changes in streamflow and continental runoff: A review. Terrestrial Water Cycle and Climate Change: Natural and Human-Induced Impacts. *Geophys Monograph*, *221*, 17–37.

Dai, A., Qian, T. T., Trenberth, K. E., & Milliman, J. D. (2009). Changes in continental freshwater discharge from 1948 to 2004. *Journal of Climate*, *22*, 2773–2792.

David, L. (2010). Cross wavelet analyses of annual continental freshwater discharge and selected climate indices. *Journal of Hydrology*, *385*(1-4), 269–278.

Davidson, E. A., de Araújo, A. C., Artaxo, P., Balch, J. K., Brown, I. F., C. Bustamante, M. M., et al. (2012). The Amazon basin in transition. *Nature*, *481*(7381), 321–328. https://doi.org/10.1038/nature10717

Delgado, J. M., Merz, B., & Apel, H. (2012). A climate-flood link for the lower Mekong River. *Hydrology and Earth System Sciences*, *16*, 1533–1541.

Döll, P., Fiedler, K., & Zhang, J. (2009). Global-scale analysis of river flow alterations due to water withdrawals and reservoirs. *Hydrology and Earth System Sciences*, *13*, 2413–2432. https://doi.org/10.5194/hess-13-24132009

Domingues, C. M., Church, J. A., White, N. J., Gleckler, P. J., Wijffels, S. E., Barker, P. M., & Dunn, J. R. (2008). Improved estimates of upper-ocean warming and multi-decadal sea-level rise. *Nature*, *453*, 1090–1093.

Enfield, D. B., Mestas-Nuñez, A. M., & Trimble, P. J. (2001). The Atlantic multidecadal oscillation and its relation to rainfall and river flows in the continental US. *Geophysical Research Letters*, *28*(10), 2077–2080. https://doi.org/10.1029/2000GL012745

Espinoza, J. C., Marengo, J. A., Ronchail, J., Carpio, J. M., Flores, L. N., & Guyot, J. L. (2014). The extreme 2014 flood in south-western Amazon basin: The role of tropical-subtropical South Atlantic SST gradient. *Environmental Research Letters*, *9*(12), 124007. https://doi.org/10.1088/1748-9326/9/12/124007

Espinoza Villar, J. C., Ronchail, J., Guyot, J. L., Cochonneau, G., Naziano, F., Lavado, W., et al. (2009). Spatio-temporal rainfall variability in the Amazon basin countries (Brazil, Peru, Bolivia, Colombia, and Ecuador). *International Journal of Climatology*, *29*(11), 1574–1594. https://doi.org/10.1002/joc.1791

Fan, H., & He, D. (2015). Temperature and precipitation variability and its effects on streamflow in the upstream regions of the Lancang–Mekong and Nu–Salween Rivers. *Jouranl of Hydrometeorology*, *16*(5), 2248–2263. https://doi.org/10.1175/JHM-D-14-0238.1

Fleming, S. W., & Dahlke, H. E. (2014). Parabolic northern-hemisphere river flow teleconnections to El Niño-Southern Oscillation and the Arctic Oscillation. *Environmental Research Letters*, *9*(10). https://doi.org/10.1088/1748-9326/9/10/104007

Foley, J. A., Botta, A., Coe, M. T., & Costa, M. H. (2002). El Niño–Southern oscillation and the climate, ecosystems and rivers of Amazonia. *Global Biogeochemical Cycles*, *16*(4), 1132. https://doi.org/10.1029/2002GB001872

Frans, C., Istanbulluoglu, E., Mishra, V., Munoz-Arriola, F., & Lettenmaier, D. P. (2013). Are climatic or land cover changes the dominant cause of runoff trends in the Upper Mississippi River Basin? *Geophysical Research Letters*, *40*, 1104–1110. https://doi.org/10.1002/grl.50262

Gedalof, Z., Peterson, D. L., & Mantua, N. J. (2004). Columbia River flow and drought since 1750. *Journal of the American Water Resources Association*, *40*(6), 1579–1592.

Gerten, D., Rost, S., von Bloh, W., & Lucht, W. (2008). Causes of change in 20th century global river discharge. *Geophysical Research Letters*, *35*, L07701. https://doi.org/10.1029/2008GL035258

Gloor, M., Brienen, R. J. W., Galbraith, D., Feldpausch, T. R., Schöngart, J., Guyot, J. L., et al. (2013). Intensification of the Amazon hydrological cycle over the last two decades. *Geophysical Research Letters*, *40*, 1729–1733. https://doi.org/10.1002/grl.50377

Gong, D., Zhu, J., & Wang, S. (2002). Significant relationship between spring AO and the summer rainfall along the Yangtze River. *Chinese Science Bulletin*, *47*(11), 948–952.

Grinsted, A., Moore, J. C., & Jevrejeva, S. (2004). Application of the cross wavelet transform and wavelet coherence to geophysical time series. *Nonlinear Processes in Geophysics*, *11*(5/6), 561–566.

Haddeland, I., Heinke, J., Biemans, H., Eisner, S., Flörke, M., Hanasaki, N., et al. (2014). Global water resources affected by human interventions and climate change. *Proceedings of the National Academy of Sciences*, *111*(9), 3251–3256. https://doi.org/10.1073/pnas.1222475110

Hodgkins, G. A., Dudley, R. W., & Huntington, T. G. (2003). Changes in the timing of high river flows in New England over the 20th century. *Journal of Hydrology*, *278*(1-4), 244–252.

Hu, W., & Si, B. C. (2013). Soil water prediction based on its scale-specific control using multivariate empirical mode decomposition. *Geoderma*, *193*, 180–188.

Hu, W., & Si, B. C. (2016). Multiple wavelet coherence for untangling scale-specific and localized multivariate relationships in geosciences. *Hydrology and Earth System Sciences*, *20*(8), 3183–3191.
Hu, W., Si, B. C., Biswas, A., & Chau, H. W. (2017). Temporally stable patterns but seasonal dependent controls of soil water content: Evidence from wavelet analyses. *Hydrological Processes*, *31*(21), 3697–3707.
Iles, C. E., & Hegerl, G. C. (2015). Systematic change in global patterns of streamflow following volcanic eruptions. *Nature Geoscience*, *8*(11), 838–842. https://doi.org/10.1038/ngeo2545
Ionita, M., Scholz, P., & Chelcea, S. (2015). Spatio-temporal variability of dryness/wetness in the Danube River Basin. *Hydrological Processes*, *29*(20), 4483–4497.
Kaiser, G. (1994). *A friendly guide to wavelets.* Boston: Birkhäuser.
Keener, V. W., Feyereisen, G. W., Lall, U., Jones, J. W., Bosch, D. D., & Lowrance, R. (2010). El-Niño/Southern Oscillation (ENSO) influences on monthly NO_3 load and concentration, stream flow and precipitation in the Little River Watershed, Tifton, Georgia (GA). *Journal of Hydrology*, *381*(3), 352–363.
Kitoh, A., Kusunoki, S., & Nakaegawa, T. (2011). Climate change projections over South America in the late 21st century with the 20 and 60 km mesh Meteorological Research Institute atmospheric general circulation model (MRI-AGCM). *Journal of Geophysical Research*, *116*, D06105. https://doi.org/10.1029/2010JD014920
Knight, J. R., Folland, C. K., & Scaife, A. A. (2006). Climate impacts of the Atlantic multidecadal oscillation. *Geophysical Research Letters*, *33*, L17706. https://doi.org/10.1029/2006GL026242
Kong, D., Miao, C., Borthwick, A. G., Duan, Q., Liu, H., Sun, Q., et al. (2015). Evolution of the Yellow River Delta and its relationship with runoff and sediment load from 1983 to 2011. *Journal of Hydrology*, *520*, 157–167.
Lavigne, M. A., Nastev, M., & Lefevbre, R. (2010). Numerical simulation of ground water flow in the Chateaugay River. *Canadian Water Resources Association Journal*, *35*, 469–486.
Lu, E., Takle, E. S., & Manoj, J. (2010). The relationships between climatic and hydrological changes in the Upper Mississippi River Basin: A SWAT and Multi-GCM study. *Journal of Hydrometeorology*, *11*(2), 437–451.
Lutz, A. F., Immerzeel, W. W., Shrestha, A. B., & Bierkens, M. F. P. (2014). Consistent increase in High Asia's runoff due to increasing glacier melt and precipitation. *Nature Climate Change*, *4*(7), 587–592.
Mallakpour, I., & Villarini, G. (2016). Investigating the relationship between the frequency of flooding over the central United States and large-scale climate. *Advances in Water Resources*, *92*, 159–171.
Maraun, D., & Kurths, J. (2004). Cross wavelet analysis: Significance testing and pitfalls. *Nonlinear Processes in Geophysics*, *11*(4), 505–514.
Marengo, J. A. (2009). Long-term trends and cycles in the hydrometeorology of the Amazon basin since the late 1920s. *Hydrological Processes*, *23*(22), 3236–3244.
Marengo, J. A., Tomasella, J., Alves, L. M., Soares, W. R., & Rodriguez, D. A. (2011). The drought of 2010 in the context of historical droughts in the Amazon region. *Geophysical Research Letters*, *38*, L12703. https://doi.org/10.1029/2011GL047436
Marengo, J. A., Tomasella, J., Soares, W. R., Alves, L. M., & Nobre, C. A. (2011). Extreme climatic events in the Amazon basin. *Theoretical and Applied Climatology*, *107*(1-2), 73–85.
Massei, N., Laignel, B., Rosero, E., Motelay-massei, A., Deloffre, J., Yang, Z. L., & Rossi, A. (2011). A wavelet approach to the short-term to pluri-decennal variability of streamflow in the Mississippi river basin from 1934 to 1998. *International Journal of Climatology*, *31*(1), 31–43.
McCabe, G. J., & Wolock, D. M. (2011). Century-scale variability in global annual runoff examined using a water balance model. *International Journal of Climatology*, *31*(12), 1739–1748.
Miao, C. Y., & Ni, J. R. (2009). Variation of natural streamflow since 1470 in the middle Yellow River China. *International Journal of Environmental Research and Public Health*, *6*(11), 2849–2864.
Mihanović, H., Orlić, M., & Pasarić, Z. (2009). Diurnal thermocline oscillations driven by tidal flow around an island in the Middle Adriatic. *Journal of Marine Systems*, *78*, S157–S168.
Milliman, J. D., & Farnsworth, K. L. (2011). *River discharge to the coastal ocean: A global synthesis*. New York: Cambridge University Press.
Milliman, J. D., Farnsworth, K. L., Jones, P. D., Xu, K. H., & Smith, L. C. (2008). Climatic and anthropogenic factors affecting river discharge to the global ocean, 1951–2000. *Global and Planetary Change*, *62*(3-4), 187–194.
Murray, S. J., Foster, P. N., & Prentice, I. C. (2012). Future global water resources with respect to climate change and water withdrawals as estimated by a dynamic global vegetation model. *Journal of Hydrology*, *448*, 14–29.
Nastev, M., Rivera, A., Lefebvre, R., Martel, R., & Savard, M. (2005). Numerical simulation of groundwater flow in regional rock aquifers, southwestern Quebec, Canada. *Hydrogeology Journal*, *13*, 835–848.
Ng, E. K. W., & Chan, J. C. L. (2012). Geophysical applications of partial wavelet coherence and multiple wavelet coherence. *Journal of Atmospheric and Oceanic Technology*, *29*, 1845–1853.
Ngo-Duc, T., Laval, K., Polcher, J., Lombard, A., & Cazenave, A. (2005). Effects of land water storage on global mean sea level over the past half century. *Geophysical Research Letters*, *32*, L09704. https://doi.org/10.1029/2005GL022719
Oki, T., Entekhabi, D., & Harrold, T. I. (2004). The global water cycle. *Washington DC American Geophysical Union Geophysical Monograph Series*, *150*, 225–237.
Oki, T., & Kanae, S. (2006). Global hydrological cycles and world water resources. *Science*, *313*, 1068–1072.
Räsänen, T. A., & Kummu, M. (2013). Spatiotemporal influences of ENSO on precipitation and flood pulse in the Mekong River Basin. *Journal of Hydrology*, *476*, 154–168.
Roudier, P., Ducharne, A., & Feyen, L. (2014). Climate change impacts on runoff in West Africa: A review. *Hydrology and Earth System Sciences*, *18*, 2789–2801.
Saeed, F., Haensler, A., Weber, T., Hagemann, S., & Jacob, D. (2013). Representation of extreme precipitation events leading to opposite climate change signals over the Congo basin. *Atmosphere*, *4*(3), 254–271.
Salas, J. D., Fu, C., & Rajagopalan, B. (2011). Long-range forecasting of Colorado streamflows based on hydrologic, atmospheric, and oceanic data. *Journal of Hydrologic Engineering*, *16*(6), 508–520.
Sanchez-Rubio, G., Perry, H. M., Biesiot, P. M., Johnson, D. R., & Lipcius, R. N. (2011). Oceanic–atmospheric modes of variability and their influence on riverine input to coastal Louisiana and Mississippi. *Journal of Hydrologic Engineering*, *396*(1-2), 72–81.
Schewe, J., Heinke, J., Gerten, D., Haddeland, I., Arnell, N. W., Clark, D. B., et al. (2014). Multimodel assessment of water scarcity under climate change. *Proceedings of the National Academy of Sciences of the United States of America*, *111*(9), 3245–3250. https://doi.org/10.1073/pnas.1222460110
Serreze, M. C., Bromwich, D. H., Clark, M. P., Etringer, A. J., Zhang, T., & Lammers, R. (2002). Large-scale hydro-climatology of the terrestrial Arctic drainage system. *Journal of Geophysical Research*, *107*(D2), 8160. https://doi.org/10.1029/2001JD000919

She, D., Cao, Y., & Chen, Q. (2016). Characterizing scale-specific environmental factors affecting soil organic carbon along two landscape transects. *Environmental Science and Pollution Research International*, *23*(18), 18,672–18,683.
Shiklomanov, A. I., & Lammers, R. B. (2014). River ice responses to a warming Arctic—Recent evidence from Russian rivers. *Environmental Research Letters*, *9*(3). https://doi.org/10.1088/1748-9326/9/3/035008
Shiklomanov, A. I., Lammers, R. B., Rawlins, M., Smith, L. C., & Pavelsky, T. M. (2007). Temporal and spatial variations in maximum river discharge from a new Russian data set. *Journal of Geophysical Research*, *112*, G04S53. https://doi.org/10.1029/2006JG000352
Si, B. C. (2008). Spatial scaling analyses of soil physical properties: A review of spectral and wavelet methods. *Vadose Zone Journal*, *7*(2), 547–562.
Sombroek, W. (2001). Spatial and temporal patterns of Amazon rainfall: Consequences for the planning of agricultural occupation and the protection of primary forests. *Ambio*, *30*(7), 388–396.
Surazakov, A. B., Aizen, V. B., Aizen, E. M., & Nikitin, S. A. (2007). Glacier changes in the Siberian Altai Mountains, Ob river basin, (1952–2006) estimated with high resolution imagery. *Environmental Research Letters*, *2*(4). https://doi.org/10.1088/1748-9326/2/4/045017
Suzuki, K., Kubota, J., Ohata, T., & Vuglinsky, V. (2006). Influence of snow ablation and frozen ground on spring runoff generation in the Mogot Experimental Watershed, southern mountainous taiga of eastern Siberia. *Hydrology Research*, *37*(1), 21–29.
Szolgayova, E., Parajka, J., Blöschl, G., & Bucher, C. (2014). Long term variability of the Danube River flow and its relation to precipitation and air temperature. *Journal of Hydrology*, *519*, 871–880.
Tang, Q., & Lettenmaier, D. P. (2012). 21st century runoff sensitivities of major global river basins. *Geophysical Research Letters*, *39*, L06403. https://doi.org/10.1029/2011GL050834
Todd, M. C., & Washington, R. (2004). Climate variability in central equatorial Africa: Influence from the Atlantic sector. *Geophysical Research Letters*, *31*, L23202. https://doi.org/10.1029/2004GL020975
Tootle, G. A., & Piechota, T. C. (2006). Relationships between Pacific and Atlantic ocean sea surface temperatures and US streamflow variability. *Water Resources Research*, *42*, W07411. https://doi.org/10.1029/2005WR004184
Tootle, G. A., Piechota, T. C., & Singh, A. (2005). Coupled oceanic-atmospheric variability and U.S. streamflow. *Water Resources Research*, *41*, W12408. https://doi.org/10.1029/2005WR004381
Torrence, C., & Compo, G. P. (1998). A practical guide to wavelet analysis. *Bulletin of the American Meteorological Society*, *79*(1), 61–78.
Trenberth, K. E. (1997). The definition of El Niño. *Bulletin of the American Meteorological Society*, *78*(12), 2771–2777.
Trenberth, K. E., Smith, L., Qian, T., Dai, A., & Fasullo, J. (2007). Estimates of the global water budget and its annual cycle using observational and model data. *Journal of Hydrometeorology*, *8*(4), 758–769.
Twine, T. E., Kucharik, C. J., & Foley, J. A. (2004). Effects of land cover change on the energy and water balance of the Mississippi River basin. *Journal of Hydrometeorology*, *5*(4), 640–655.
Twine, T. E., Kucharik, C. J., & Foley, J. A. (2005). Effects of El Niño–Southern Oscillation on the climate, water balance, and streamflow of the Mississippi River basin. *Journal of Climate*, *18*(22), 4840–4861.
Van der Ent, R. J., Savenije, H. H., Schaefli, B., & Steele-Dunne, S. C. (2010). Origin and fate of atmospheric moisture over continents. *Water Resources Research*, *46*, W09525. https://doi.org/10.1029/2010WR009127
Vorosmarty, C. J., Green, P., Salisbury, J., & Lammers, R. B. (2000). Global water resources: Vulnerability from climate change and population growth. *Science*, *289*(5477), 284–288. https://doi.org/10.1126/science.289.5477.284
Wanders, N., & Wada, Y. (2015). Decadal predictability of river discharge with climate oscillations over the 20th and early 21st century. *Geophysical Research Letters*, *42*, 10,689–10,695. https://doi.org/10.1002/2015GL066929
Wang, Y., Tong, J., Xu, C., & Shi, Y. (2006). Trend of evapotranspiration over the Yangtze River Basin in 1961-2000. *Advances in Climate Change Research*, *2*(S1), 35–40.
Weber, M., Braun, L., Mauser, W., & Prasch, M. (2010). Contribution of rain, snow-and icemelt in the Upper Danube discharge today and in the future. *Geografia Fisica e Dinamica Quaternaria*, *33*(2), 221–230.
Wei, W., Chang, Y., & Dai, Z. (2014). Streamflow changes of the Changjiang (Yangtze) River in the recent 60 years: Impacts of the East Asian summer monsoon, ENSO, and human activities. *Quaternary International*, *336*, 98–107.
Xu, K., Milliman, J. D., & Xu, H. (2010). Temporal trend of precipitation and runoff in major Chinese Rivers since 1951. *Global and Planetary Change*, *73*(3-4), 219–232.
Xu, K. H., Milliman, J. D., Yang, Z. S., & Xu, H. (2007). Climatic and anthropogenic impacts on the water and sediment discharge from the Yangtze River (Changjiang), 1950–2005. *Large rivers: Geomorphology and management*, 609–626. https://doi.org/10.1002/9780470723722.ch29
Yang, S. L., Liu, Z., Dai, S. B., Gao, Z. X., Zhang, J., Wang, H. J., et al. (2010). Temporal variations in water resources in the Yangtze River (Changjiang) over the Industrial Period based on reconstruction of missing monthly discharges. *Water Resources Research*, *46*, W10516. https://doi.org/10.1029/2009WR008589
Yang, T., Asanjan, A., Welles, E., Gao, X., Sorooshian, S., & Liu, X. (2017). Developing reservoir monthly inflow forecasts using artificial intelligence and climate phenomenon information. *Water Resources Research*, *53*, 2786–2812. https://doi.org/10.1002/2017WR020482
Yang, T., Gao, X., Sorooshian, S., & Li, X. (2016). Simulating California reservoir operation using the classification and regression-tree algorithm combined with a shuffled cross-validation scheme. *Water Resources Research*, *52*, 1626–1651. https://doi.org/10.1002/2015WR017394
Yang, Y., Jia, X., Wendroth, O., Liu, B., Shi, Y., Huang, T., & Bai, X. (2019). Noise-assisted multivariate empirical mode decomposition of saturated hydraulic conductivity along a south-north transect across the Loess Plateau of China. *Soil Science Society of America Journal*. https://doi.org/10.2136/sssaj2018.11.0438
Yu, S., Yang, J., Liu, G., Yao, R., & Wang, X. (2015). Improvement for the multi-scale periodic characteristics revealing of precipitation signals and its impact assessment on soil hydrological process by combining HHT and CWT approaches. *Natural Hazards and Earth System Sciences*, *15*(3), 393–407.
Zeng, N., Yoon, J. H., Marengo, J. A., Subramaniam, A., Nobre, C. A., Mariotti, A., & Neelin, J. D. (2008). Causes and impacts of the 2005 Amazon drought. *Environmental Research Letters*, *3*(1). https://doi.org/10.1088/1748-9326/3/1/014002
Zhang, Q., Jiang, T., Gemmer, M., & Becker, S. (2005). Precipitation, temperature and runoff analysis from 1950 to 2002 in the Yangtze basin China. *Hydrological Sciences Journal*, *50*(1), 65–80.
Zhang, X., Fan, D., Wang, H., & Yang, Z. (2014). Water discharge variability of Changjiang (Yangtze) and Huanghe (Yellow) Rivers and its response to climatic changes. *Chinese Journal of Oceanology and Limnology*, *32*(6), 1392–1405.
Zhang, Y., Wallace, J. M., & Battisti, D. S. (1997). ENSO-like interdecadal variability: 1900-93. *Journal of Climate*, *10*(5), 1004–1020.
Zhang, Y. K., & Schilling, K. E. (2006). Increasing streamflow and baseflow in Mississippi River since the 1940s: Effect of land use change. *Journal of Hydrology*, *324*(1-4), 412–422.